

# Data analysis of gravitational-wave signals from spinning neutron stars.

## II. Accuracy of estimation of parameters

Piotr Jaranowski<sup>1,2</sup>

Andrzej Królak<sup>1,3</sup>

<sup>1</sup>*Albert-Einstein-Institut, Max-Planck-Institut für Gravitationsphysik  
Schlaatzweg 1, 14473 Potsdam, Germany*

<sup>2</sup>*Institute of Physics, Białystok University  
Lipowa 41, 15-424 Białystok, Poland*

<sup>3</sup>*Institute of Mathematics, Polish Academy of Sciences  
Śniadeckich 8, 00-950 Warsaw, Poland*

July 30, 2018

### Abstract

We examine the accuracy of estimation of parameters of the gravitational-wave signals from spinning neutron stars that can be achieved from observations by Earth-based laser interferometers. We consider a model of the signal consisting of two narrowband components and including both phase and amplitude modulation. We calculate approximate values of the rms errors of the parameter estimators using the Fisher information matrix. We carry out extensive Monte Carlo simulations and obtain cumulative distribution functions of rms errors of astrophysically interesting parameters: amplitude of the signal, wobble angle, position of the source in the sky, frequency, and spindown coefficients. We consider both all-sky searches and directed searches. We also examine the possibility of determination of neutron star proper motion. We perform simulations for all laser-interferometric detectors that are currently under construction and for several possible lengths of the observation time and sizes of the parameter space. We find that observations of continuous gravitational-wave signals from neutron stars by laser-interferometric detectors will provide a very accurate information about their astrophysical properties. We derive several simplified models of the signal that can be used in the theoretical investigations of the data analysis schemes independently of the physical mechanisms generating the gravitational-wave signal.

## 1 Introduction

Detection of gravitational waves from spinning neutron stars by currently constructed long-arm laser interferometers [1, 2, 3, 4] is expected to provide a wealth of astrophysical information about these objects. In the first paper of this series [5] (hereafter Paper I) we introduced a model of the gravitational-wave signal from a spinning neutron star. The response of a laser interferometer to such a signal will carry information about the neutron star period of rotation and its evolution, amplitude of the signal and its polarization. Moreover even the response of a single detector will contain the full information about the position of the source in the sky. Also higher order terms in the phase contain velocity of the source and its distance. In this second paper of our series we investigate in detail how accurately these astrophysically interesting parameters can be determined from observations by laser-interferometric detectors. We assume that optimal data analysis methods presented in Paper I are used. We use a standard tool, the Fisher information matrix, to assess the rms errors of our estimation method.

We find impressive potential accuracies achievable with gravitational-wave detectors that can make them into astronomical laboratories competitive with optical and radio observatories. For all-sky searches and 120 days of observation time the initial laser-interferometric detectors will be able to locate the strongest fast and young neutron star gravitational-wave emitters at a distance of 1 kpc with accuracy of order  $10^{-7}$  sr and estimate the frequency and the four spindown parameters of the wave with relative accuracies of order  $10^{-2(4-k)}$ , where  $k = 0, \dots, 4$  denotes the  $k$ th spindown ( $k = 0$  corresponds to the frequency of the wave). Amplitude can be estimated within a few percent and wobble angle within a few percent of a radian. For directed searches the relative rms errors of estimation of frequency and spindowns will decrease with respect to the all-sky searches by a factor of 10 for the fourth spindown,

$10^2$  for the third and the second spindowns,  $10^3$  for the first spindown, and  $10^4$  for the frequency. With advanced detectors a reasonable accuracy of estimation of proper motions of neutron stars with all-sky searches will be achievable for nearby neutron stars (at distances of 40 pc or so).

The plan of the paper is as follows. In Sec. 2 we review the model of the gravitational-wave signal introduced in Paper I. We introduce eight special cases of the model depending on whether observation time is long or short and neutron star is young or old and it is spinning fast or slow. In Sec. 3 we present calculations of the rms errors that can be achieved for our models assuming that we use maximum likelihood detection as data analysis method. To estimate the rms errors we use Fisher information matrix. In Sec. 4 we explore the possibility of estimating proper motion of neutron stars from gravitational-wave observations. In Sec. 5 we introduce a number of simplified signal models that enable us to assess the rms errors of the phase parameters independently of the physical mechanisms generating the gravitational radiation from a spinning neutron star. In Sec. 6 using a simplified model we investigate the dependence of the rms errors of the parameters on the observational parameters: duration of observation, initial moment of observation and the latitude of the detector.

Several additional topics are investigated in the appendices. In Appendix A we interpret our 1/4 of a cycle criterion in terms of the signal-to-noise ratio loss. In Appendix B we give details of number of cycles calculations for our special models. In Appendix C we study the polynomial phase model and the effect of the choice of the initial time in the parameter estimation problem.

## 2 A model of the two-component gravitational-wave signal

In Sec. II of Paper I we have introduced the following two-component model of the gravitational-wave signal  $h$  from a spinning neutron star:

$$h(t) = h_1(t) + h_2(t), \quad (1)$$

with

$$h_1(t) = F_+(t)h_{1+}(t) + F_\times(t)h_{1\times}(t), \quad h_2(t) = F_+(t)h_{2+}(t) + F_\times(t)h_{2\times}(t), \quad (2)$$

$$h_{1+}(t) = \frac{1}{8}h_o \sin 2\theta \sin 2\iota \cos \Psi(t), \quad h_{2+}(t) = \frac{1}{2}h_o \sin^2 \theta (1 + \cos^2 \iota) \cos 2\Psi(t), \quad (3)$$

$$h_{1\times}(t) = \frac{1}{4}h_o \sin 2\theta \sin \iota \sin \Psi(t), \quad h_{2\times}(t) = h_o \sin^2 \theta \cos \iota \sin 2\Psi(t). \quad (4)$$

The model of the signal given above represents the quadrupole gravitational wave that is emitted by a freely precessing axisymmetric star. The angle  $\theta$ , called the wobble angle, is the angle between the total angular momentum vector of the star and the star's axis of symmetry and  $\iota$  is the angle between the total angular momentum vector of the star and the direction from the star to the Earth. For the case when  $\theta = \pi/2$  (then the component  $h_1$  vanishes) the model also gives the quadrupole wave from a triaxial ellipsoid rotating about a principal axis. In both cases the amplitude  $h_o$  is given by

$$h_o = \frac{16\pi^2 G}{c^4} \frac{\epsilon I f_o^2}{r_o}, \quad (5)$$

where  $I$  is the moment of inertia with respect to the rotation axis and  $r_o$  is the distance to the star. For precessing axisymmetric star  $f_o$  is the sum of the frequency of rotation of the star and the frequency of precession and  $\epsilon$  is the poloidal ellipticity of the star whereas for triaxial ellipsoid  $f_o$  is the frequency of rotation of the star and  $\epsilon$  is ellipticity of the star defined by  $\epsilon := (I_1 - I_2)/I$ , where  $I_1$  and  $I_2$  are the moments of inertia of the star with respect to the principal axes orthogonal to the rotation axis.

Inserting numerical values into Eq. (5) gives

$$h_o = 4.23 \times 10^{-25} d_o \left( \frac{f_o}{100 \text{ Hz}} \right)^2, \quad (6)$$

where

$$d_o := \frac{\epsilon}{10^{-5}} \frac{I}{10^{45} \text{ g cm}^2} \frac{1 \text{ kpc}}{r_o}. \quad (7)$$

In all numerical simulations presented in the next sections except for the case when the effect of the proper motion was studied we had assumed the numerical value of the parameter  $d_o$  to be 1. The most uncertain parameter in Eq. (7) is the ellipticity  $\epsilon$ , the value of  $\epsilon \sim 10^{-5}$  is thought to be an upper limit and typical values may be significantly less [6].

The beam-pattern functions  $F_+$  and  $F_\times$  from Eq. (2) are given by

$$F_+(t) = \sin \zeta [a(t) \cos 2\psi + b(t) \sin 2\psi], \quad (8)$$

$$F_\times(t) = \sin \zeta [b(t) \cos 2\psi - a(t) \sin 2\psi], \quad (9)$$

where

$$\begin{aligned}
a(t) &= \frac{1}{16} \sin 2\gamma (3 - \cos 2\lambda) (3 - \cos 2\delta) \cos[2(\alpha - \phi_r - \Omega_r t)] \\
&\quad - \frac{1}{4} \cos 2\gamma \sin \lambda (3 - \cos 2\delta) \sin[2(\alpha - \phi_r - \Omega_r t)] \\
&\quad + \frac{1}{4} \sin 2\gamma \sin 2\lambda \sin 2\delta \cos[\alpha - \phi_r - \Omega_r t] \\
&\quad - \frac{1}{2} \cos 2\gamma \cos \lambda \sin 2\delta \sin[\alpha - \phi_r - \Omega_r t] \\
&\quad + \frac{3}{4} \sin 2\gamma \cos^2 \lambda \cos^2 \delta,
\end{aligned} \tag{10}$$

$$\begin{aligned}
b(t) &= \cos 2\gamma \sin \lambda \sin \delta \cos[2(\alpha - \phi_r - \Omega_r t)] \\
&\quad + \frac{1}{4} \sin 2\gamma (3 - \cos 2\lambda) \sin \delta \sin[2(\alpha - \phi_r - \Omega_r t)] \\
&\quad + \cos 2\gamma \cos \lambda \cos \delta \cos[\alpha - \phi_r - \Omega_r t] \\
&\quad + \frac{1}{2} \sin 2\gamma \sin 2\lambda \cos \delta \sin[\alpha - \phi_r - \Omega_r t].
\end{aligned} \tag{11}$$

The angles  $\alpha$ ,  $\delta$ , and  $\psi$  are respectively right ascension, declination of the gravitational-wave source, and polarization angle (these angles determine the orientation of the wave reference frame with respect to the celestial sphere reference frame). The angle  $\lambda$  is the latitude of the detector's site,  $\gamma$  determines the orientation of the detector's arms with respect to local geographical directions and  $\zeta$  is the angle between the interferometer arms.  $\Omega_r$  is the rotational angular velocity of the Earth, and  $\phi_r$  is a deterministic phase which defines the position of the Earth in its diurnal motion at  $t = 0$ . The derivation of the formulae (8)–(11) is given in Sec. II A of Paper I.

The phase  $\Psi$  of Eqs. (3) and (4) is given by

$$\Psi(t) = \Phi_0 + 2\pi \sum_{k=0}^{s_1} \frac{f_o^{(k)} t^{k+1}}{(k+1)!} + \frac{2\pi}{c} \mathbf{n}_0 \cdot \mathbf{r}_{\text{ES}}(t) \sum_{k=0}^{s_2} \frac{f_o^{(k)} t^k}{k!} + \frac{2\pi}{c} \mathbf{n}_0 \cdot \mathbf{r}_{\text{E}}(t) \sum_{k=0}^{s_3} \frac{f_o^{(k)} t^k}{k!}, \tag{12}$$

where  $\mathbf{r}_{\text{ES}}$  is the vector joining the solar system barycenter (SSB) with the center of the Earth and  $\mathbf{r}_{\text{E}}$  joins the center of the Earth with the detector,  $f_o^{(k)}$  is the  $k$ th time derivative of the instantaneous frequency at the SSB evaluated at  $t = 0$ ,  $\mathbf{n}_0$  is the constant unit vector in the direction of the star in the SSB reference frame. We have neglected the relativistic effects. To derive the above model we assumed that in the rest frame of the neutron star the gravitational-wave frequency can be expanded in a power series. For the detailed derivation of the phase model (12) see Sec. II B and Appendix A of Paper I.

Neglecting the eccentricity of the Earth's orbit and the motion of the Earth around the Earth-Moon barycenter the scalar products  $\mathbf{n}_0 \cdot \mathbf{r}_{\text{E}}$  and  $\mathbf{n}_0 \cdot \mathbf{r}_{\text{ES}}$  of Eq. (12) can be written as (see Sec. II B of Paper I)

$$\mathbf{n}_0 \cdot \mathbf{r}_{\text{E}} = R_E [\sin \lambda \sin \delta + \cos \lambda \cos \delta \cos(\alpha - \phi_r - \Omega_r t)], \tag{13}$$

$$\mathbf{n}_0 \cdot \mathbf{r}_{\text{ES}} = R_{\text{ES}} [\cos \alpha \cos \delta \cos(\phi_o + \Omega_o t) + (\cos \varepsilon \sin \alpha \cos \delta + \sin \varepsilon \sin \delta) \sin(\phi_o + \Omega_o t)], \tag{14}$$

where  $R_{\text{ES}} = 1$  AU is the mean distance from the Earth's center to the SSB,  $R_E$  is the mean radius of the Earth,  $\Omega_o$  is the mean orbital angular velocity of the Earth, and  $\phi_o$  is a deterministic phase which defines the position of the Earth in its orbital motion at  $t = 0$ ,  $\varepsilon$  is the angle between ecliptic and the Earth's equator.

The extremal values of the spindown parameters  $f_o^{(k)}$  are estimated from the formula

$$f_o^{(k)} \simeq (-1)^k k! \frac{f_o}{\tau^k}, \quad k = 1, 2, \dots, \tag{15}$$

where  $\tau$  we call the spindown age of the star.

We choose the number of terms in the power series on the right-hand side of Eq. (12) according to the following criterion: *we exclude an effect from the model of the signal in the case when it contributes less than 1/4 of a cycle to the phase of the signal during the observation time.* An interpretation of the 1/4 of a cycle criterion in terms of the signal-to-noise ratio loss is given in Appendix A. If we restrict to observation times  $T_o \leq 120$  days, frequencies  $f_o \leq 1000$  Hz, and spindown ages  $\tau \geq 40$  years, the phase model (12) meets the criterion for an appropriate choice of the numbers  $s_1$ ,  $s_2$ , and  $s_3$ . Also the effect of the star proper motion in the phase is negligible if we assume that the star moves w.r.t. the SSB not faster than  $10^3$  km/s and its distance to the Earth  $r_o \geq 1$  kpc. However for nearby neutron stars at distances  $r_o \geq 40$  pc the proper motion contribution to the phase (12) can exceed 1/4 of a cycle. We discuss this issue at the end of the present section.

$T_o$ (days)	$\tau_{\min}$ (years)	$f_{g\max}$ (Hz)	$s_1$	$s_2$	$s_3$
120	40	$10^3$	4	3	0
120	40	200	4	2	0
120	$10^3$	$10^3$	2	1	0
120	$10^3$	200	2	1	0
7	40	$10^3$	2	1	0
7	40	200	2	1	0
7	$10^3$	$10^3$	1	1	0
7	$10^3$	200	1	1	0

Table 1: The number of spindown terms needed in various contributions to the phase of the signal depending on the type of population of neutron stars searched for. The number  $s_1$  refers to the spindown contribution,  $s_2$  refers to the Earth orbital motion, and  $s_3$  refers to the Earth diurnal motion contribution [cf. Eq. (12)].

We consider several models depending on the range of the gravitational-wave frequency  $f_g$  [ $f_g = f_o$  for the  $h_1$  component and  $f_g = 2f_o$  for the  $h_2$  component of the signal (1)], spindown age  $\tau$ , and observation time  $T_o$ . Following Brady *et al.* [6] we say that neutron star is *slow* if  $f_g \simeq 200$  Hz and *fast* if  $f_g \simeq 1$  kHz. We define a neutron star to be *old* if  $\tau \simeq 10^3$  yr and *young* if  $\tau \simeq 40$  yr. We consider observation time to be *short* if  $T_o \simeq 7$  days and *long* if  $T_o \simeq 120$  days. Accordingly we have eight possible models. In Table 1 we present the number of terms needed in the power series of various contributions to the phase in order to meet the above criterion. The details of the calculation are given in Appendix B.

In our calculations of the rms errors of the estimators of the parameters we have also studied the case of directed searches. By directed searches we mean the search for the signal from a spinning neutron star which position in the sky is known. This reduces the dimension of the parameter space by 2 since the right ascension and the declination of the source are known. We do not assume that the gravitational wave frequency is known. Even if we are searching for a gravitational wave from a known pulsar its frequency may not coincide with the frequency of the electromagnetic radiation or be exactly twice that frequency. For directed searches the values of the parameters  $s_1$ ,  $s_2$ , and  $s_3$  given in Table 1 remain in general the same however for specific positions in the sky they may be less.

The numbers of spindowns that must be included in the phase model given in Table 1 agree with the corresponding numbers of Brady *et al.* [6] obtained by a different criterion for the cases they considered (see Figure 6 of their paper).

We have also considered the effect of the proper motion of the neutron star on the phase of the signal assuming that it moves uniformly with respect to the SSB reference frame. We have found that for the observation time  $T_o = 120$  days and the extreme case of a neutron star at a distance  $r_o = 40$  pc, transverse velocity  $|\mathbf{v}_{\text{ns}\perp}| = 10^3$  km/s (where  $\mathbf{v}_{\text{ns}\perp}$  is the component of the star's velocity  $\mathbf{v}_{\text{ns}}$  perpendicular to the vector  $\mathbf{n}_0$ ), gravitational-wave frequency  $f_g = 2f_o = 1$  kHz, and spindown age  $\tau = 40$  years, proper motion contributes only  $\sim 4$  cycles to the phase of the signal. This dominant proper motion contribution  $\Psi_{\text{pm}}$  to the phase (12) is given by (cf. Eq. (A20) in Appendix A of Paper I)

$$\Psi_{\text{pm}}(t) = \frac{2\pi}{c} \frac{\mathbf{v}_{\text{ns}\perp} \cdot \mathbf{r}_{\text{ES}}(t)}{r_o} f_o t. \quad (16)$$

The ratio  $\mathbf{v}_{\text{ns}\perp}/r_o$  determines the proper motion of the star. We shall study the accuracy of estimation of the proper motion in Sec. 4.

### 3 Estimation of parameters of the two-component signal

In Sec. III of Paper I we have presented an optimum data analysis method: *maximum likelihood detection*. This method consists of maximizing the likelihood function  $\Lambda$  with respect to the parameters of the signal. If the maximum of  $\Lambda$  exceeds a certain threshold calculated from the false alarm probability that we can afford we say that the signal is detected. The values of the parameters that maximize  $\Lambda$  are said to be the *maximum likelihood estimators* of the parameters of the signal. Let us collect the signal parameters into the vector  $\boldsymbol{\theta} = (\theta_1, \dots, \theta_n)$ . The covariance matrix  $C$  of the estimators of the parameters  $\boldsymbol{\theta}$  is approximately given by the inverse of the *Fisher information matrix*  $\Gamma$ :  $C \cong \Gamma^{-1}$ . This approximation is the better the higher the signal-to-noise ratio. For a signal  $h$  buried in a Gaussian noise the components of the Fisher matrix  $\Gamma$  are given by

$$\Gamma_{ij} = \left( \frac{\partial h}{\partial \theta_i} \middle| \frac{\partial h}{\partial \theta_j} \right), \quad (17)$$

where the scalar product  $(\cdot | \cdot)$  is defined by

$$(x|y) := 4\Re \int_0^\infty \frac{\tilde{x}(f)\tilde{y}^*(f)}{S_h(f)} df, \quad (18)$$

where  $\tilde{\cdot}$  denotes the Fourier transform,  $*$  is complex conjugation, and  $S_h$  is the *one-sided* spectral density of the detector's noise.

For a signal  $h = h_1 + h_2$  that consists of two narrowband components around the frequencies  $f_o$  ( $h_1$  component) and  $2f_o$  ( $h_2$  component), assuming that over the bandwidth of the signal the noise spectral density  $S_h$  is nearly constant and equal to  $S_h(f_o)$  or  $S_h(2f_o)$ , the Fisher matrix  $\Gamma$  is approximately given by

$$\Gamma_{ij} \cong \frac{2}{S_h(f_o)} \int_{-T_o/2}^{T_o/2} \frac{\partial h_1}{\partial \theta_i} \frac{\partial h_1}{\partial \theta_j} dt + \frac{2}{S_h(2f_o)} \int_{-T_o/2}^{T_o/2} \frac{\partial h_2}{\partial \theta_i} \frac{\partial h_2}{\partial \theta_j} dt, \quad (19)$$

where  $T_o$  is the observation time and the observation interval is  $[-T_o/2, T_o/2]$ .

For the two-component signal defined by Eqs. (1)–(4) we can extract explicitly the dependence of the elements of the covariance matrix  $C$  on the amplitude parameter  $h_o$ . Let us write the signal (1) in the form

$$h(t; \boldsymbol{\theta}) = h_o [\chi_1(t; \boldsymbol{\zeta}) + \chi_2(t; \boldsymbol{\zeta})], \quad (20)$$

where  $\boldsymbol{\theta} = (h_o, \boldsymbol{\zeta})$ , i.e.  $\boldsymbol{\zeta}$  is the vector of all the signal parameters with the exception of  $h_o$ . Let us note that  $\boldsymbol{\zeta} = (\alpha, \delta, \psi, \iota, \theta, \Phi_0, f_o^{(1)}, f_o^{(s)}, \dots, f_o^{(s)})$ , so the signal (20) depends on  $8 + s$  parameters, where  $s$  is the number of the spindowns one wants to include. Substituting Eq. (20) into (19) one can show that the components of the covariance matrix  $C \cong \Gamma^{-1}$  can be written using the matrix notation as (superscript  $T$  denotes matrix transposition):

$$C_{h_o h_o} \cong K, \quad (21)$$

$$C_{h_o \boldsymbol{\zeta}} \cong -\frac{1}{h_o} K \Delta' (\Delta'')^{-1}, \quad (22)$$

$$C_{\boldsymbol{\zeta} \boldsymbol{\zeta}} \cong \frac{1}{h_o^2} [(\Delta'')^{-1} + K (\Delta'')^{-1} (\Delta')^T \Delta' (\Delta'')^{-1}], \quad (23)$$

where

$$K := [\Delta - \Delta' (\Delta'')^{-1} (\Delta')^T]^{-1}, \quad (24)$$

$$\Delta := \frac{2}{S_h(f_o)} \int_{-T_o/2}^{T_o/2} [\chi_1(t; \boldsymbol{\zeta})]^2 dt + \frac{2}{S_h(2f_o)} \int_{-T_o/2}^{T_o/2} [\chi_2(t; \boldsymbol{\zeta})]^2 dt, \quad (25)$$

$$\Delta'_i := \frac{2}{S_h(f_o)} \int_{-T_o/2}^{T_o/2} \chi_1(t; \boldsymbol{\zeta}) \frac{\partial \chi_1(t; \boldsymbol{\zeta})}{\partial \zeta_i} dt + \frac{2}{S_h(2f_o)} \int_{-T_o/2}^{T_o/2} \chi_2(t; \boldsymbol{\zeta}) \frac{\partial \chi_2(t; \boldsymbol{\zeta})}{\partial \zeta_i} dt, \quad (26)$$

$$\Delta''_{ij} := \frac{2}{S_h(f_o)} \int_{-T_o/2}^{T_o/2} \frac{\partial \chi_1(t; \boldsymbol{\zeta})}{\partial \zeta_i} \frac{\partial \chi_1(t; \boldsymbol{\zeta})}{\partial \zeta_j} dt + \frac{2}{S_h(2f_o)} \int_{-T_o/2}^{T_o/2} \frac{\partial \chi_2(t; \boldsymbol{\zeta})}{\partial \zeta_i} \frac{\partial \chi_2(t; \boldsymbol{\zeta})}{\partial \zeta_j} dt. \quad (27)$$

The optimal signal-to-noise ratio  $d := \sqrt{(h|h)}$  for the signal (20) can be computed from the formula (cf. Sec. III C of Paper I):

$$d^2 \cong \frac{2h_o^2}{S_h(f_o)} \int_{-T_o/2}^{T_o/2} [\chi_1(t; \boldsymbol{\zeta})]^2 dt + \frac{2h_o^2}{S_h(2f_o)} \int_{-T_o/2}^{T_o/2} [\chi_2(t; \boldsymbol{\zeta})]^2 dt. \quad (28)$$

We have used the formulae (21)–(27) to calculate numerically covariance matrices for different phase models. Because the components of the covariance matrices depend in a complicated way on the trigonometric functions of the angles  $\alpha$ ,  $\delta$ ,  $\psi$ ,  $\iota$ , and  $\theta$  we have resorted to the Monte Carlo simulations. For each simulation of a covariance matrix we have generated 1000 sets of the angles  $\{\alpha, \delta, \psi, \iota, \theta\}$  according to the probability measure

$$d\alpha \times d\sin \delta \times d\psi \times d\cos \iota \times d\theta$$

defined on the parameter space

$$\{\alpha \in [0, 2\pi), \sin \delta \in [-1, 1], \psi \in [0, 2\pi), \cos \iota \in [-1, 1], \theta \in [0, \pi]\}.$$

In the simulations we have assumed the following models of the noise spectral densities  $S_h$  in the individual detectors. The noise curves for the VIRGO and the initial/advanced LIGO detectors are adopted from [7], and the noise curve for the TAMA300 detector is taken from [4, 8]. Wideband and narrowband versions of the GEO600 detector noise are based on [9].

We present results of the simulations by plotting the cumulative distribution functions for the square roots of the diagonal components of the covariance matrix which approximate the rms errors of the estimators of the parameters. For some cases we also give tables with quartiles of the distributions [10]. We study the rms errors (denoted by  $\sigma$ ) of the following astrophysically important parameters: amplitude  $h_o$ , wobble angle  $\theta$ , position of the source on the sky, frequency  $f_o$ , and spindown parameters  $f_o^{(k)}$ . The accuracy of the position on the sky is measured by the solid angle  $\Delta\Omega$  corresponding to the ellipse of semiaxes  $\sigma(\delta)$  and  $\sigma(\alpha)$  and is given by

$$\Delta\Omega = \pi \cos \delta \sigma(\delta) \sigma(\alpha). \quad (29)$$

To assess the relative rms errors of the spindown parameters  $f_o^{(k)}$  we have assumed in the simulations the extremal values of these parameters given by formula (15).

In Figure 1 we have given cumulative distributions for the rms errors of the parameters for all the laser-interferometric detectors under construction. For the GEO600 detector we have also considered the narrowband configuration tuned to 1 kHz with bandwidth of 30 Hz. We have taken long observation time ( $T_o = 120$  days) and we have assumed the neutron star to be fast ( $f_o = 500$  Hz) and young ( $\tau = 40$  yr). In addition in Table 2 we have given the quartiles of the distributions plotted in Figure 1. We observe that the rms errors for the case of advanced detectors are 10 times less than for the initial detectors. This is a result of simplified assumptions for the spectral density of shot noise for the advanced detectors, namely it is taken exactly 100 times less than for the initial detectors (for frequency range of 500 Hz to 1 kHz the shot noise dominates).

The GEO600 detector in narrowband configuration tuned to a certain frequency (1 kHz in this case) is able to achieve accuracies of estimation of parameters in the phase of the signal (position on the sky, frequency and spindown parameters) several times better than kilometer-length initial detectors. This is done at the expense of loss of information at other frequency bands. We see that the accuracy of the estimation of the amplitude  $h_o$  and the angle  $\theta$  for the narrowband case is less than for any other detector. This is because the narrowband GEO600 detector will see mainly one component of the signal ( $h_2$  in this case) where parameters  $h_o$  and  $\theta$  degenerate into one parameter. The information about the other component is small resulting in a small accuracy for joint estimation of parameters  $h_o$  and  $\theta$ . It implies that for the narrowband GEO600 detector it is more suitable to model the signal as consisting only of the second ( $h_2$ ) component. Then the parameters  $h_o$  and  $\theta$  merge into an effective amplitude parameter  $h'_o = h_o \sin^2 \theta$  [cf. Eqs. (1)–(4)]. We have performed the Monte Carlo simulations for this case. On the left top panel in Figure 1 we have shown the cumulative distribution function for the relative rms error of the amplitude  $h'_o$ . We have checked that the position error  $\Delta\Omega$  and the spindown relative errors  $\sigma(f_o^{(k)})/|f_o|$  ( $k = 0, \dots, 4$ ) are almost the same as for the case of the two-component signal model indicating negligible contribution of the first component ( $h_1$ ) to the information about the phase parameters.

From Table 2 we see that the initial laser-interferometric gravitational-wave detectors will be able to locate the strongest fast and young neutron star gravitational-wave emitters at a distance of 1 kpc with accuracy of order  $10^{-7}$  sr and estimate the relative accuracies of frequency ( $k = 0$ ) and four spindowns ( $k = 1, \dots, 4$ ) within a factor of order  $10^{-2(4-k)}$ . Amplitude can be estimated within a few percent and angle  $\theta$  within a few percent of a radian.

In Figures 2 and 3 we have performed the Monte Carlo simulations of the rms parameter errors for the eight models of the phase summarized in Table 1 above. Figure 2 is for long observation time  $T_o = 120$  days and Figure 3 is for short observation time  $T_o = 7$  days. Because the amplitude of the signal for our model increases as square of the frequency [see Eq. (5)] the rms errors of the parameters for fast rotating stars are smaller than for slowly rotating ones. For the case of young neutron stars the spindowns are larger than for the old ones [see Eq. (15)] and this leads to more spindown terms in the phase for young stars in order to meet the 1/4 of a cycle criterion (see Table 1). Since spindown parameters are strongly correlated (see Appendix C) increasing their number decreases the accuracy of their estimation. Thus accuracies for estimation of parameters for young neutron stars tend to be less than for the old ones.

We observe that the accuracy of estimation of the phase parameters (except for the fourth spindown  $f_o^{(4)}$ ) is in all cases very good. The distributions of the rms errors of the amplitude parameters  $h_o$  and  $\theta$  for various distinct models of the phase in the case when the frequency  $f_o$  and consequently the amplitude  $h_o$  is the same are indistinguishable (see top panels of Figures 2 and 3). This shows that the amplitude parameters and the phase parameters in our signal model are effectively uncorrelated.

In Figures 4–6 and Table 3 we have presented results of the same simulations as in Figures 1–3 and Table 2 but for directed searches. Here because there are two unknown parameters less in the phase of the signal (the right ascension  $\alpha$  and the declination  $\delta$  are assumed to be known) the accuracy of estimation of the phase parameters increases. For the initial detectors the relative rms errors of the frequency ( $k = 0$ ) and the first two spindowns ( $k = 1, 2$ ) are of the order of  $10^{-3(4-k)}$ , and the relative rms errors

detector		$\frac{\sigma(h_o)}{h_o}$	$\sigma(\theta)$ (rad)	$\Delta\Omega$ (sr)	$\frac{\sigma(f_o)}{f_o}$	$\frac{\sigma(f_o)}{ f_o }^{(1)}$	$\frac{\sigma(f_o)}{ f_o }^{(2)}$	$\frac{\sigma(f_o)}{ f_o }^{(3)}$	$\frac{\sigma(f_o)}{ f_o }^{(4)}$	$d$
GEO600 wideband noise	$q_{0.25}$	$4.3 \times 10^{-2}$	$3.5 \times 10^{-2}$	$1.1 \times 10^{-6}$	$5.3 \times 10^{-8}$	$6.4 \times 10^{-6}$	$1.7 \times 10^{-3}$	$6.4 \times 10^{-2}$	8.5	17
	$q_{0.5}$	$9.0 \times 10^{-2}$	$6.6 \times 10^{-2}$	$3.6 \times 10^{-6}$	$9.8 \times 10^{-8}$	$1.0 \times 10^{-5}$	$3.1 \times 10^{-3}$	$1.0 \times 10^{-1}$	16	28
	$q_{0.75}$	$5.2 \times 10^{-1}$	$1.7 \times 10^{-1}$	$2.4 \times 10^{-5}$	$2.6 \times 10^{-7}$	$2.2 \times 10^{-5}$	$8.2 \times 10^{-3}$	$2.2 \times 10^{-1}$	42	37
GEO600 narrowband noise	$q_{0.25}$	$2.0 \times 10^{-1}$	$2.2 \times 10^{-1}$	$1.7 \times 10^{-8}$	$6.6 \times 10^{-9}$	$7.7 \times 10^{-7}$	$2.1 \times 10^{-4}$	$7.7 \times 10^{-3}$	1.1	47
	$q_{0.5}$	$5.3 \times 10^{-1}$	$2.6 \times 10^{-1}$	$7.1 \times 10^{-8}$	$1.4 \times 10^{-8}$	$1.3 \times 10^{-6}$	$4.5 \times 10^{-4}$	$1.3 \times 10^{-2}$	2.3	160
	$q_{0.75}$	1.5	$3.0 \times 10^{-1}$	$8.4 \times 10^{-7}$	$5.1 \times 10^{-8}$	$4.5 \times 10^{-6}$	$1.6 \times 10^{-3}$	$4.5 \times 10^{-2}$	8.2	280
initial Hanford	$q_{0.25}$	$1.3 \times 10^{-2}$	$1.1 \times 10^{-2}$	$7.9 \times 10^{-8}$	$1.4 \times 10^{-8}$	$1.8 \times 10^{-6}$	$4.5 \times 10^{-4}$	$1.9 \times 10^{-2}$	2.3	56
	$q_{0.5}$	$2.8 \times 10^{-2}$	$2.0 \times 10^{-2}$	$2.6 \times 10^{-7}$	$2.6 \times 10^{-8}$	$2.9 \times 10^{-6}$	$8.1 \times 10^{-4}$	$2.9 \times 10^{-2}$	4.1	96
	$q_{0.75}$	$1.5 \times 10^{-1}$	$5.1 \times 10^{-2}$	$1.8 \times 10^{-6}$	$6.9 \times 10^{-8}$	$6.2 \times 10^{-6}$	$2.2 \times 10^{-3}$	$6.3 \times 10^{-2}$	11	120
advanced Hanford	$q_{0.25}$	$1.3 \times 10^{-3}$	$1.1 \times 10^{-3}$	$7.9 \times 10^{-10}$	$1.4 \times 10^{-9}$	$1.8 \times 10^{-7}$	$4.5 \times 10^{-5}$	$1.8 \times 10^{-3}$	0.23	560
	$q_{0.5}$	$2.8 \times 10^{-3}$	$2.0 \times 10^{-3}$	$2.6 \times 10^{-9}$	$2.6 \times 10^{-9}$	$2.9 \times 10^{-7}$	$8.1 \times 10^{-5}$	$2.9 \times 10^{-3}$	0.41	960
	$q_{0.75}$	$1.5 \times 10^{-2}$	$5.0 \times 10^{-3}$	$1.7 \times 10^{-8}$	$6.9 \times 10^{-9}$	$6.2 \times 10^{-7}$	$2.2 \times 10^{-4}$	$6.3 \times 10^{-3}$	1.1	1200
initial Livingston	$q_{0.25}$	$1.2 \times 10^{-2}$	$1.0 \times 10^{-2}$	$6.2 \times 10^{-8}$	$1.3 \times 10^{-8}$	$1.8 \times 10^{-6}$	$4.0 \times 10^{-4}$	$1.8 \times 10^{-2}$	2.0	58
	$q_{0.5}$	$2.7 \times 10^{-2}$	$2.0 \times 10^{-2}$	$1.8 \times 10^{-7}$	$2.2 \times 10^{-8}$	$2.7 \times 10^{-6}$	$7.0 \times 10^{-4}$	$2.7 \times 10^{-2}$	3.6	97
	$q_{0.75}$	$1.4 \times 10^{-1}$	$4.7 \times 10^{-2}$	$1.1 \times 10^{-6}$	$5.7 \times 10^{-8}$	$5.8 \times 10^{-6}$	$1.8 \times 10^{-3}$	$5.8 \times 10^{-2}$	9.1	120
advanced Livingston	$q_{0.25}$	$1.2 \times 10^{-3}$	$1.0 \times 10^{-3}$	$6.2 \times 10^{-10}$	$1.3 \times 10^{-9}$	$1.8 \times 10^{-7}$	$4.0 \times 10^{-5}$	$1.8 \times 10^{-3}$	0.20	580
	$q_{0.5}$	$2.7 \times 10^{-3}$	$1.9 \times 10^{-3}$	$1.8 \times 10^{-9}$	$2.2 \times 10^{-9}$	$2.7 \times 10^{-7}$	$7.0 \times 10^{-5}$	$2.7 \times 10^{-3}$	0.35	970
	$q_{0.75}$	$1.4 \times 10^{-2}$	$4.7 \times 10^{-3}$	$1.1 \times 10^{-8}$	$5.7 \times 10^{-9}$	$5.7 \times 10^{-7}$	$1.8 \times 10^{-4}$	$5.8 \times 10^{-3}$	0.91	1200
VIRGO	$q_{0.25}$	$1.1 \times 10^{-2}$	$9.6 \times 10^{-3}$	$5.6 \times 10^{-8}$	$1.2 \times 10^{-8}$	$1.5 \times 10^{-6}$	$3.8 \times 10^{-4}$	$1.6 \times 10^{-2}$	1.9	57
	$q_{0.5}$	$2.5 \times 10^{-2}$	$1.8 \times 10^{-2}$	$1.8 \times 10^{-7}$	$2.2 \times 10^{-8}$	$2.4 \times 10^{-6}$	$6.9 \times 10^{-4}$	$2.5 \times 10^{-2}$	3.5	100
	$q_{0.75}$	$1.3 \times 10^{-1}$	$4.4 \times 10^{-2}$	$1.3 \times 10^{-6}$	$6.1 \times 10^{-8}$	$5.9 \times 10^{-6}$	$1.9 \times 10^{-3}$	$5.9 \times 10^{-2}$	9.7	140
TAMA300	$q_{0.25}$	$1.2 \times 10^{-1}$	$1.2 \times 10^{-1}$	$4.6 \times 10^{-7}$	$3.6 \times 10^{-8}$	$4.7 \times 10^{-6}$	$1.1 \times 10^{-3}$	$4.7 \times 10^{-2}$	5.7	17
	$q_{0.5}$	$3.0 \times 10^{-1}$	$1.5 \times 10^{-1}$	$1.8 \times 10^{-6}$	$7.4 \times 10^{-8}$	$7.8 \times 10^{-6}$	$2.3 \times 10^{-3}$	$7.9 \times 10^{-2}$	12	33
	$q_{0.75}$	1.3	$3.1 \times 10^{-1}$	$2.0 \times 10^{-5}$	$2.4 \times 10^{-7}$	$2.5 \times 10^{-5}$	$7.4 \times 10^{-3}$	$2.6 \times 10^{-1}$	38	46

Table 2: The quartiles [10] for the Monte Carlo simulated distributions of the rms errors of the signal parameters for the individual detectors in the case of all-sky searches. The observation time  $T_o = 120$  days. The neutron star parameters are the same as in Figure 1, the frequency  $f_o = 500$  Hz, and the spindown age  $\tau = 40$  years. The model of the signal's phase is described by  $s_1 = 4$ ,  $s_2 = 3$ , and  $s_3 = 0$  (cf. Table 1). The dimensionless amplitude of the waveform is  $h_o = 1.1 \times 10^{-23}$ . For the GEO600 detector we use two noise curves: wideband and narrowband tuned to 1 kHz with the bandwidth of 30 Hz. The last column shows the quartiles of the Monte Carlo simulated distributions of the signal-to-noise ratio  $d$  [given by Eq. (28)], it is taken from Table II of Paper I.

of the third and the fourth spindown are of the order  $10^{-4}$  and  $10^{-1}$ , respectively. This gives a decrease with respect to the all-sky searches by factors of  $10^4$ ,  $10^3$ ,  $10^2$ ,  $10^2$ , and 10 for the frequency, the first, the second, the third, and the fourth spindown respectively. Again the distributions of the rms errors of the amplitude parameters  $h_o$  and  $\theta$  for the models with the same frequency  $f_o$  are indistinguishable (see top panels of Figures 5 and 6). Moreover the distributions in the top panels of Figures 2 and 3 (all-sky searches) are indistinguishable from the corresponding distributions in Figures 5 and 6 (directed searches). Since the signal model for all-sky searches and the corresponding model for directed searches differ only in the number of the unknown parameters in the phase of the signal this confirms an effective decorrelation of the amplitude and the phase parameters. This fact will enable us (in Sec. 6 below) to give an assessment of the rms errors of the phase parameters independently of the physical mechanisms generating the gravitational waves from a spinning neutron star.

## 4 Estimation of the proper motion of the neutron star

To describe the proper motion of the neutron star we shall introduce the parameters that are customarily used by the pulsar astronomers. When the star moves with respect to the SSB reference frame its right ascension  $\alpha$  and declination  $\delta$  change. To first order we can assume that they change linearly with time, i.e. we have

$$\alpha = \alpha_0 + \mu_\alpha t, \quad \delta = \delta_0 + \mu_\delta t. \quad (30)$$

Let us denote by  $\mathbf{v}_{\text{ns}}$  the velocity of the star w.r.t. the SSB reference frame and by  $\mathbf{v}_{\text{ns}\perp}$  the component of the velocity  $\mathbf{v}_{\text{ns}}$  perpendicular to the unit vector  $\mathbf{n}_0$  in the direction of the star ( $\mathbf{n}_0$  is along the line of

detector		$\frac{\sigma(h_o)}{h_o}$	$\sigma(\theta)$ (rad)	$\frac{\sigma(f_o)}{f_o}$	$\frac{\sigma(f_o)}{ f_o }^{(1)}$	$\frac{\sigma(f_o)}{ f_o }^{(2)}$	$\frac{\sigma(f_o)}{ f_o }^{(3)}$	$\frac{\sigma(f_o)}{ f_o }^{(4)}$	$d$
GEO600 wideband noise	$q_{0.25}$	$4.3 \times 10^{-2}$	$3.4 \times 10^{-2}$	$6.7 \times 10^{-12}$	$5.0 \times 10^{-9}$	$4.7 \times 10^{-6}$	$6.7 \times 10^{-4}$	0.40	17
	$q_{0.5}$	$8.8 \times 10^{-2}$	$6.6 \times 10^{-2}$	$1.1 \times 10^{-11}$	$8.0 \times 10^{-9}$	$7.4 \times 10^{-6}$	$1.1 \times 10^{-3}$	0.64	28
	$q_{0.75}$	$5.0 \times 10^{-1}$	$1.7 \times 10^{-1}$	$2.3 \times 10^{-11}$	$1.7 \times 10^{-8}$	$1.6 \times 10^{-5}$	$2.3 \times 10^{-3}$	1.4	37
GEO600 narrowband noise	$q_{0.25}$	$2.0 \times 10^{-1}$	$2.2 \times 10^{-1}$	$8.0 \times 10^{-13}$	$6.0 \times 10^{-10}$	$5.6 \times 10^{-7}$	$8.0 \times 10^{-5}$	0.048	47
	$q_{0.5}$	$5.3 \times 10^{-1}$	$2.6 \times 10^{-1}$	$1.4 \times 10^{-12}$	$1.0 \times 10^{-9}$	$9.6 \times 10^{-7}$	$1.4 \times 10^{-4}$	0.083	160
	$q_{0.75}$	1.5	$3.0 \times 10^{-1}$	$4.6 \times 10^{-12}$	$3.5 \times 10^{-9}$	$3.2 \times 10^{-6}$	$4.6 \times 10^{-4}$	0.28	280
initial Hanford	$q_{0.25}$	$1.3 \times 10^{-2}$	$1.1 \times 10^{-2}$	$2.0 \times 10^{-12}$	$1.5 \times 10^{-9}$	$1.4 \times 10^{-6}$	$2.0 \times 10^{-4}$	0.12	56
	$q_{0.5}$	$2.8 \times 10^{-2}$	$2.0 \times 10^{-2}$	$3.1 \times 10^{-12}$	$2.4 \times 10^{-9}$	$2.2 \times 10^{-6}$	$3.1 \times 10^{-4}$	0.19	96
	$q_{0.75}$	$1.5 \times 10^{-1}$	$5.1 \times 10^{-2}$	$6.7 \times 10^{-12}$	$5.1 \times 10^{-9}$	$4.7 \times 10^{-6}$	$6.7 \times 10^{-4}$	0.41	120
advanced Hanford	$q_{0.25}$	$1.3 \times 10^{-3}$	$1.1 \times 10^{-3}$	$2.0 \times 10^{-13}$	$1.5 \times 10^{-10}$	$1.4 \times 10^{-7}$	$2.0 \times 10^{-5}$	0.012	560
	$q_{0.5}$	$2.8 \times 10^{-3}$	$2.0 \times 10^{-3}$	$3.1 \times 10^{-13}$	$2.3 \times 10^{-10}$	$2.2 \times 10^{-7}$	$3.1 \times 10^{-5}$	0.019	960
	$q_{0.75}$	$1.5 \times 10^{-2}$	$5.1 \times 10^{-3}$	$6.7 \times 10^{-13}$	$5.0 \times 10^{-10}$	$4.7 \times 10^{-7}$	$6.7 \times 10^{-5}$	0.040	1200
initial Livingston	$q_{0.25}$	$1.2 \times 10^{-2}$	$1.0 \times 10^{-2}$	$2.0 \times 10^{-12}$	$1.5 \times 10^{-9}$	$1.4 \times 10^{-6}$	$2.0 \times 10^{-4}$	0.12	58
	$q_{0.5}$	$2.6 \times 10^{-2}$	$2.0 \times 10^{-2}$	$3.0 \times 10^{-12}$	$2.3 \times 10^{-9}$	$2.1 \times 10^{-6}$	$3.0 \times 10^{-4}$	0.18	97
	$q_{0.75}$	$1.4 \times 10^{-2}$	$4.7 \times 10^{-2}$	$6.7 \times 10^{-12}$	$5.0 \times 10^{-9}$	$4.6 \times 10^{-6}$	$6.6 \times 10^{-4}$	0.40	120
advanced Livingston	$q_{0.25}$	$1.2 \times 10^{-3}$	$1.0 \times 10^{-3}$	$2.0 \times 10^{-13}$	$1.5 \times 10^{-10}$	$1.4 \times 10^{-7}$	$2.0 \times 10^{-5}$	0.012	580
	$q_{0.5}$	$2.6 \times 10^{-3}$	$1.9 \times 10^{-3}$	$3.0 \times 10^{-13}$	$2.3 \times 10^{-10}$	$2.1 \times 10^{-7}$	$3.0 \times 10^{-5}$	0.018	970
	$q_{0.75}$	$1.4 \times 10^{-2}$	$4.7 \times 10^{-3}$	$6.6 \times 10^{-13}$	$5.0 \times 10^{-10}$	$4.6 \times 10^{-7}$	$6.6 \times 10^{-5}$	0.040	1200
VIRGO	$q_{0.25}$	$1.1 \times 10^{-2}$	$9.5 \times 10^{-3}$	$1.7 \times 10^{-12}$	$1.3 \times 10^{-9}$	$1.2 \times 10^{-6}$	$1.7 \times 10^{-4}$	0.10	57
	$q_{0.5}$	$2.5 \times 10^{-2}$	$1.8 \times 10^{-2}$	$2.6 \times 10^{-12}$	$2.0 \times 10^{-9}$	$1.8 \times 10^{-6}$	$2.6 \times 10^{-4}$	0.16	100
	$q_{0.75}$	$1.4 \times 10^{-1}$	$4.4 \times 10^{-2}$	$6.4 \times 10^{-12}$	$4.8 \times 10^{-9}$	$4.5 \times 10^{-6}$	$6.4 \times 10^{-4}$	0.39	140
TAMA300	$q_{0.25}$	$1.2 \times 10^{-1}$	$1.2 \times 10^{-1}$	$5.2 \times 10^{-12}$	$3.9 \times 10^{-9}$	$3.6 \times 10^{-6}$	$5.2 \times 10^{-4}$	0.31	17
	$q_{0.5}$	$3.0 \times 10^{-1}$	$1.5 \times 10^{-1}$	$8.8 \times 10^{-12}$	$6.6 \times 10^{-9}$	$6.1 \times 10^{-6}$	$8.8 \times 10^{-4}$	0.53	33
	$q_{0.75}$	1.3	$3.0 \times 10^{-1}$	$2.8 \times 10^{-11}$	$2.1 \times 10^{-8}$	$2.0 \times 10^{-5}$	$2.8 \times 10^{-3}$	1.7	46

Table 3: The quartiles [10] for the Monte Carlo simulated distributions of the rms errors of the signal parameters for the individual detectors in the case when the position of the source in the sky is known. The observation time  $T_o = 120$  days. The neutron star parameters are the same as in Figure 1, the frequency  $f_o = 500$  Hz, and the spindown age  $\tau = 40$  years. The model of the signal's phase is described by  $s_1 = 4$ ,  $s_2 = 3$ , and  $s_3 = 0$  (cf. Table 1). The dimensionless amplitude of the waveform is  $h_o = 1.1 \times 10^{-23}$ . For the GEO600 detector we use two noise curves: wideband and narrowband tuned to 1 kHz with the bandwidth of 30 Hz. The last column shows the quartiles of the Monte Carlo simulated distributions of the signal-to-noise ratio  $d$  [given by Eq. (28)], it is taken from Table II of Paper I.

sight to the star at  $t = 0$  for the observer located in the SSB). To first order in time it is easy to express the velocity  $\mathbf{v}_{\text{ns}\perp}$  in terms of the parameters  $\mu_\alpha$  and  $\mu_\delta$ . We have

$$\mathbf{v}_{\text{ns}\perp} = r_o \begin{pmatrix} -\mu_\alpha \sin \alpha_0 \cos \delta_0 - \mu_\delta \cos \alpha_0 \sin \delta_0 \\ \mu_\alpha \cos \alpha_0 \cos \delta_0 - \mu_\delta \sin \alpha_0 \sin \delta_0 \\ \mu_\delta \cos \delta_0 \end{pmatrix}. \quad (31)$$

The total proper motion of the star  $\mu := |\mathbf{v}_{\text{ns}\perp}|/r_o$  is given in terms of  $\mu_\alpha$  and  $\mu_\delta$  as follows:

$$\mu = \sqrt{\mu_\delta^2 + \mu_\alpha^2 \cos^2 \delta_0}. \quad (32)$$

In our Monte Carlo simulation we have considered the extreme case of a nearby neutron star at a distance of 40 pc. We have taken the transverse velocity  $|\mathbf{v}_{\text{ns}\perp}|$  of the star to be  $10^3$  km/s. Careful modelling of the pulsar statistics has shown that the pulsar velocities extend to these values [11, 12]. For  $|\mathbf{v}_{\text{ns}\perp}| = 10^3$  km/s and  $r_o = 40$  pc the contribution (16) to the phase due to the proper motion is  $\sim 4$  cycles for frequency  $f_o = 500$  Hz (this value we have used in the simulation) and it decreases linearly with distance.

One can show that in the extreme case we consider here the phase model consistent with the 1/4 of a cycle criterion for 120 days of observation time and young neutron star with spindown age  $\tau = 40$  years reads [cf. Eqs. (12) and (16)]

$$\Psi(t) = \Phi_0 + 2\pi \sum_{k=0}^4 f_o \frac{t^{k+1}}{(k+1)!} + \frac{2\pi}{c} \mathbf{n}_o \cdot \mathbf{r}_{\text{ES}}(t) \sum_{k=0}^3 f_o \frac{t^k}{k!} + \frac{2\pi}{c} \left( \mathbf{n}_o \cdot \mathbf{r}_{\text{E}}(t) + \frac{\mathbf{v}_{\text{ns}\perp} \cdot \mathbf{r}_{\text{ES}}(t)}{r_o} t \right) f_o. \quad (33)$$



For the phase given by Eq. (33) the two-component gravitational-wave signal defined by Eqs. (1)–(4) depends on the following 14 parameters:  $h_o, \alpha_0, \mu_\alpha, \delta_0, \mu_\delta, \psi, \iota, \theta, \Phi_0, f_o, f_o^{(1)}, \dots, f_o^{(4)}$ .

In the Monte Carlo simulation for each set of randomly generated angles  $\{\alpha_0, \delta_0, \psi, \iota, \theta\}$  we have also randomly chosen the direction of the star’s motion on the sky keeping the total proper motion  $\mu$  of the star fixed and equal to  $(10^3 \text{ km/s})/(40 \text{ pc}) \cong 5.3 \times 10^3 \text{ mas/yr}$  (mas/yr stands for milliarcseconds per year, units usually used in pulsar astronomy).

The results of the numerical simulations are summarized in Figure 7. We have assumed Hanford LIGO detector in the advanced configuration and 120 days of observation time. The extreme case considered here gives interesting accuracies of the estimation of the proper motion parameters resulting in the median of the distributions of  $\sigma(\mu_\alpha)$  and  $\sigma(\mu_\delta)$  to be  $\sim 2 \times 10^3 \text{ mas/yr}$  (i.e. 40% rms error). As the distance to the source is small the estimation of the fourth spindown parameter  $f_o^{(4)}$  with a good accuracy of  $\sim 10\%$  is also possible.

## 5 Simplified models of the gravitational-wave signal

The phase of the gravitational-wave signal from a spinning neutron star changes at the detector on the Earth over a characteristic time of less than 100 ms whereas the amplitude of the signal changes over one day. This means that the detection of a long continuous signal requires an accurate model for its phase. As shown in Appendix A even 1/4 of a cycle difference between the filter and the signal can lead to loss of the signal-to-noise ratio by 10%.

Accurate modelling of the amplitude is not so crucial. Consequently the information on the phase parameters in the amplitudes of the signal is much smaller than in the phase. This can clearly be seen from our simulations presented in Sec. 3 which show that the phase parameters can be estimated much more accurately than the amplitude parameters (see Figures 1 to 6). As a result the phase parameters effectively decorrelate from the amplitude parameters. This decorrelation is shown in our numerical simulations (see discussion at the end of Sec. 3 and Figures 2, 3, 5, 6, see also Figure 15). Therefore we can expect to obtain a model of a signal with constant amplitudes (i.e. with no amplitude modulation) that reproduces the covariance matrix for the phase parameters of the full signal. Such a model is presented in Sec. 5.1 below.

We also find it useful to have a *linear parametrization* of the phase of the signal i.e. a set of parameters such that the phase is a linear function of the parameters. One advantage of the linear parametrization is that the maximum likelihood estimators of the parameters are unbiased [14]. The other property of a linearly parametrized phase is that the covariance matrix is independent of the values of the parameters. In real data analysis schemes optimization of the codes when using a linear parametrization would be independent of the values of the parameters, i.e. of the parameter region searched. We find that the linear parametrization is not possible in general. In Sec. 5.2 we show however that it can be achieved approximately by neglecting a term in the phase arising from Earth diurnal motion and all contributions from the spindowns in the Earth spin and orbital terms.

In Sec. 5.3 we present another linear model (called linear model II) that has been investigated by one of us [15]. It is obtained by neglecting completely Earth diurnal motion and all spindowns in Earth orbital motion terms. The simplest, polynomial in time phase model, is introduced in Sec. 5.4. In this model the motion of the detector w.r.t. the SSB is ignored. In Sec. 5.5 we describe the results of Monte Carlo simulations of the covariance matrix to compare the simplified models of the signal with the exact two-component model given in Sec. 2.

### 5.1 Constant amplitude model

The constant amplitude model of the gravitational-wave signal has the phase of the exact model whereas the time dependent amplitudes are replaced by some constant effective values. We have obtained these effective values from the analytic formula for the signal-to-noise ratio given in Appendix B of Paper I. The signal-to-noise ratio consists of a term proportional to the square root of the observation time and some oscillatory term. For the observation times longer than several days the term proportional to the square root of the observation time strongly dominates. Our effective amplitudes take into account only this dominant part of the signal-to-noise ratio. Thus for the two-component signal  $h$  that we consider the constant amplitude model depends on the two constant amplitudes  $h_{o1}$  and  $h_{o2}$  as well as on the two initial phase parameters  $\Phi_{01}$  and  $\Phi_{02}$ :

$$h(t) = h_{o1} \sin[\Phi(t) + \Phi_{01}] + h_{o2} \sin[2\Phi(t) + \Phi_{02}], \quad (34)$$

where the phase  $\Phi$  coincides with the exact phase model given by Eq. (12). The constant amplitudes  $h_{o1}$  and  $h_{o2}$  read [cf. Eqs. (85), (86), and Appendix B in Paper I]

$$h_{o1} = h_o \sin \zeta |\sin 2\theta| \sqrt{F_1(\iota) e_1(\delta) \cos 4\psi + G_1(\iota) e_2(\delta)}, \quad (35)$$

$$h_{o2} = h_o \sin \zeta \sin^2 \theta \sqrt{F_2(\iota) e_1(\delta) \cos 4\psi + G_2(\iota) e_2(\delta)}, \quad (36)$$

where

$$\begin{aligned} F_1(\iota) &= -\frac{1}{16} \sin^4 \iota, & F_2(\iota) &= \frac{1}{4} \sin^4 \iota, \\ G_1(\iota) &= \frac{1}{16} \sin^2 \iota (1 + \cos^2 \iota), & G_2(\iota) &= \frac{1}{4} (1 + 6 \cos^2 \iota + \cos^4 \iota), \\ e_1(\delta) &= 4j_1 \cos^4 \delta, & e_2(\delta) &= 4j_2 - j_3 \cos 2\delta + j_1 \cos^2 2\delta, \\ j_1 &= \frac{1}{256} (4 - 20 \cos^2 \lambda + 35 \sin^2 2\gamma \cos^4 \lambda), \\ j_2 &= \frac{1}{1024} (68 - 20 \cos^2 \lambda - 13 \sin^2 2\gamma \cos^4 \lambda), \\ j_3 &= \frac{1}{128} (28 - 44 \cos^2 \lambda + 5 \sin^2 2\gamma \cos^4 \lambda). \end{aligned}$$

## 5.2 Linear model I

The signal  $h'$  of the linear model I has two constant amplitudes given by Eqs. (35) and (36) so it can be written as

$$h'(t) = h_{o1} \sin[\Phi'(t) + \Phi_{01}] + h_{o2} \sin[2\Phi'(t) + \Phi_{02}]. \quad (37)$$

The phase  $\Phi'$  of the signal  $h'$  differs from the exact phase model  $\Phi$  given by Eq. (12) by neglecting all spindowns in the phase modulation due to the orbital motion of the Earth and by discarding the component of the vector  $\mathbf{r}_d$  defining the position of the detector w.r.t. the SSB which is perpendicular to the ecliptic (see Sec.2.2 of Paper I). The function  $\Phi'$  is thus given by

$$\begin{aligned} \Phi'(t) &= 2\pi \sum_{k=0}^s f_o^{(k)} \frac{t^{k+1}}{(k+1)!} \\ &+ \frac{2\pi f_o}{c} \{(\cos \varepsilon \sin \alpha \cos \delta + \sin \varepsilon \sin \delta) [R_{ES} \sin(\phi_o + \Omega_o t) + R_E \cos \lambda \cos \varepsilon \sin(\phi_r + \Omega_r t)] \\ &+ \cos \alpha \cos \delta [R_{ES} \cos(\phi_o + \Omega_o t) + R_E \cos \lambda \cos(\phi_r + \Omega_r t)]\}. \end{aligned} \quad (38)$$

After introducing the two new parameters

$$\alpha_1 := f_o (\cos \varepsilon \sin \alpha \cos \delta + \sin \varepsilon \sin \delta), \quad \alpha_2 := f_o \cos \alpha \cos \delta, \quad (39)$$

the phase (38) becomes a linear function of the new parameters  $f_o^{(1)}$ ,  $f_o^{(s)}$ ,  $\alpha_1$ , and  $\alpha_2$ .

## 5.3 Linear model II

For the linear model II the signal  $h''$  is defined by

$$h''(t) = h_{o1} \sin[\Phi''(t) + \Phi_{01}] + h_{o2} \sin[2\Phi''(t) + \Phi_{02}], \quad (40)$$

where again the constant amplitudes  $h_{o1}$  and  $h_{o2}$  are given by Eqs. (35) and (36). In the phase  $\Phi''$  of the signal compared with the exact phase model  $\Phi$  given by Eq. (12) we neglect all spindowns in the phase modulation due to the orbital motion of the Earth and we discard the whole modulation due to the Earth's diurnal motion. The function  $\Phi''$  is thus given by

$$\begin{aligned} \Phi''(t) &= 2\pi \sum_{k=0}^s f_o^{(k)} \frac{t^{k+1}}{(k+1)!} \\ &+ \frac{2\pi f_o}{c} R_{ES} [\cos \alpha \cos \delta \cos(\phi_o + \Omega_o t) + (\cos \varepsilon \sin \alpha \cos \delta + \sin \varepsilon \sin \delta) \sin(\phi_o + \Omega_o t)]. \end{aligned} \quad (41)$$

As in the previous model after introducing the parameters

$$\alpha_1 := f_o (\cos \varepsilon \sin \alpha \cos \delta + \sin \varepsilon \sin \delta), \quad \alpha_2 := f_o \cos \alpha \cos \delta, \quad (42)$$

the phase (41) becomes a linear function of the parameters  $f_o^{(1)}$ ,  $f_o^{(s)}$ ,  $\alpha_1$ , and  $\alpha_2$ .

A version of the above model including only the second component was used in a simplified study of data analysis of gravitational-wave signals from spinning neutron stars made by one of the authors [15].

Let us observe that both the constant amplitude model of Sec. 5.1 and the linear model I of Sec. 5.2 coincide with the linear model II for a detector located at the north or the south pole (then  $\lambda = \pm 90^\circ$ ).

## 5.4 Polynomial model

In this model the signal  $h'''$  is given by

$$h'''(t) = h_{o1} \sin[\Phi'''(t) + \Phi_{01}] + h_{o2} \sin[2\Phi'''(t) + \Phi_{02}], \quad (43)$$

with the constant amplitudes  $h_{o1}$  and  $h_{o2}$  defined by Eqs. (35) and (36). In the phase  $\Phi'''$  of the signal (43) we discard all the terms due to the motion of the detector relative to the SSB. This leads to the following polynomial in time model of the phase

$$\Phi'''(t) = 2\pi \sum_{k=0}^s f_o \frac{t^{k+1}}{(k+1)!}. \quad (44)$$

For the case of directed searches i.e. when the position of the source in the sky is known, the phase is a linear function of the unknown parameters: initial phase, frequency, and spindowns and thus the exact phase model is linear. In Sec. 5.5 below we find that for directed searches the polynomial model reproduces accurately the covariance matrix for the exact model. We investigate the polynomial phase model in more detail in Appendix C.

## 5.5 Simplified models vs. the exact model

We have carried out the Monte Carlo simulations to compare our simplified signal models with the exact model given in Sec. 2. In our comparisons we have considered both all-sky searches and directed searches and we have chosen two observation times: 7 days and 120 days. We have found that the constant amplitude model of Sec. 5.1 reproduces very accurately the results of the exact model (see Figures 8 and 9 for results of Monte Carlo simulations). Also the linear model I reproduces the rms errors of the exact model well (see Figures 8 and 9). We have compared the percentiles of the distributions of the rms errors of the phase parameters for this model with the percentiles of the distributions of the exact model. We have found that for all-sky searches and observation time of 7 days, frequency  $f_o = 500$  Hz, and spindown age  $\tau = 40$  years, the maximum differences for various parameters range from  $\sim 15\%$  to  $\sim 60\%$ . For observation time of 120 days and the same frequency and spindown age the corresponding differences range from  $\sim 7\%$  to  $\sim 50\%$ . For the linear model II the deviations of the rms errors from the exact model are large (see Figures 8 and 9).

We have found that for directed searches the polynomial phase model introduced in Sec. 5.4 reproduces the results of the exact model very well. For observation time of 7 days the maximum percentile differences of the distributions of the phase parameter errors are around 5% and for observation time of 120 days they are less than 1%.

Numerical calculations of the covariance matrices for the constant amplitude models are enormously simplified compared to the amplitude modulated signals. Since the model of the phase is independent of the physical mechanisms generating the gravitational radiation, the simpler constant amplitude models characterize well a general continuous gravitational-wave signal and they can be a useful tool in theoretical analysis of the gravitational-wave signals from spinning neutron stars. However we cannot compromise the detectability of signals for simplicity of the constant amplitude and linear phase models and we do not insist on using them in real data analysis schemes. Nonetheless for searches over certain limited parameter space or for shorter observation times the simplified models (both constant amplitude and linear phase models) may be useful.

## 6 Dependence of the covariance matrix on the observational parameters

It is clear that covariance matrices of various signals considered in the present paper depend on the observation time  $T_o$ . We also notice that the phases of our signals and consequently the covariance matrices depend also on the deterministic phases  $\phi_o$ ,  $\phi_r$  and on the latitude  $\lambda$  of the detector's location [see Eqs. (12)–(14)]. The values of the phases  $\phi_o$  and  $\phi_r$  depend on the initial time of the observation. It is important to know these dependencies and therefore we study them in detail in this section.

The results of the previous section indicate that the constant amplitude linear phase model of Sec. 5.2 reproduces well the covariance matrices of the exact model. For directed searches even the simpler polynomial model of Sec. 5.4 is adequate. Therefore we adopt these two models to study the dependence of covariance matrices on  $T_o$ ,  $\phi_o$ ,  $\phi_r$ , and  $\lambda$ . Moreover we restrict ourselves to the one-component versions of these models.

Both models of Sec. 5.2 and of Sec. 5.4 are the constant amplitude models. We first derive the general formulae for the covariance matrix valid for the constant amplitude signal with any phase model, provided the signal is narrowband around some frequency  $f_o$ . Such a one-component signal can be written as

$$h(t; h_o, \zeta) = h_o \sin \Psi(t; \zeta), \quad (45)$$

where  $h_o$  is a constant amplitude and  $\zeta$  denotes parameters entering the phase  $\Psi$  of the signal. We collect all the signal parameters into the vector  $\theta = (h_o, \zeta)$ . Assuming that over the bandwidth of the signal the spectral density  $S_h$  of the noise is nearly constant and equal to  $S_h(f_o)$  and that during the observation time the phase  $\Psi$  has many cycles the optimal signal-to-noise ratio  $d := \sqrt{(h|h)}$  for the signal (45) equals

$$d \cong \frac{h_o \sqrt{T_o}}{\sqrt{S_h(f_o)}}. \quad (46)$$

The Fisher matrix  $\Gamma$  for that signal can be written as [cf. Eq. (19)]:

$$\Gamma_{\theta_i \theta_j} \cong \frac{2}{S_h(f_o)} \int_{-T_o/2}^{T_o/2} \frac{\partial h}{\partial \theta_i} \frac{\partial h}{\partial \theta_j} dt, \quad (47)$$

where  $T_o$  is the observation time and the observation interval is  $[-T_o/2, T_o/2]$ . The components of the matrix  $\Gamma$  read:

$$\Gamma_{h_o h_o} \cong \frac{d^2}{h_o^2}, \quad (48)$$

$$\Gamma_{h_o \zeta_i} \cong 0, \quad (49)$$

$$\Gamma_{\zeta_i \zeta_j} \cong d^2 \tilde{\Gamma}_{\zeta_i \zeta_j}, \quad (50)$$

where the reduced Fisher matrix  $\tilde{\Gamma}$  is defined by

$$\tilde{\Gamma}_{\zeta_i \zeta_j} := \frac{1}{T_o} \int_{-T_o/2}^{T_o/2} \frac{\partial \Psi}{\partial \zeta_i} \frac{\partial \Psi}{\partial \zeta_j} dt. \quad (51)$$

The covariance matrix  $C$  approximated by the inverse of the Fisher matrix  $\Gamma$  has the components

$$C_{h_o h_o} \cong \frac{h_o^2}{d^2}, \quad (52)$$

$$C_{h_o \zeta_i} \cong 0, \quad (53)$$

$$C_{\zeta_i \zeta_j} \cong \frac{1}{d^2} \left( \tilde{\Gamma}^{-1} \right)_{\zeta_i \zeta_j}. \quad (54)$$

It is sometimes convenient to replace the spindowns  $f_o$  by the dimensionless parameters  $\omega_k$  defined as

$$\omega_k := \frac{2\pi}{(k+1)!} f_o^{(k)} T_o^{k+1}, \quad (55)$$

where  $T_o$  is the observation time. The rms errors of the spindown parameters  $f_o^{(k)}$  are related to the rms errors of the dimensionless parameters  $\omega_k$  by

$$\sigma(f_o^{(k)}) = \frac{(k+1)!}{2\pi} \frac{1}{T_o^{k+1}} \sigma(\omega_k), \quad k = 0, \dots, s. \quad (56)$$

The significance of the parameters  $\omega_k$  can be explained as follows. In the polynomial phase model (discussed in Appendix C) the covariance matrix for the parameters  $\omega_k$  is independent of the observation time  $T_o$ , so it is completely determined by the number of spindowns included in the phase. In all more complicated phase models considered in this paper, including the exact phase model introduced in Sec. 2, the phase is the sum of the polynomial in time part and extra terms due to the motion of the detector w.r.t. the SSB. The polynomial part gives dominant contribution to the number of cycles in the phase and it roughly determines how the covariance matrices depend on the observation time  $T_o$ . Using the parameters  $\omega_k$  instead of  $f_o^{(k)}$  we absorb the polynomial phase model dependence on  $T_o$  into the very definition of the parameters  $\omega_k$ . If the covariance matrix for the parameters  $\omega_k$  in a non-polynomial phase model depends on  $T_o$ , this dependence is a measure of how this model is different from the polynomial phase model.

For all-sky searches we have studied the dependence of covariance matrices on  $T_o$ ,  $\phi_r$ ,  $\phi_o$ , and  $\lambda$  using the constant amplitude linear phase signal of Sec. 5.2. We have rewritten the phase of this signal in terms

of the parameters (39) and (55) (then the phase is a linear function of these parameters). The signal can be written as [cf. Eq. (38)]

$$h(t; h_o, \zeta) = h_o \sin \Psi(t; \zeta), \quad (57)$$

$$\begin{aligned} \Psi(t; \zeta) = & \Phi_0 + \sum_{k=0}^s \omega_k \left( \frac{t}{T_o} \right)^{k+1} + \frac{2\pi}{c} \{ \alpha_1 [R_{ES} \sin(\phi_o + \Omega_o t) + R_E \cos \lambda \cos \varepsilon \sin(\phi_r + \Omega_r t)] \\ & + \alpha_2 [R_{ES} \cos(\phi_o + \Omega_o t) + R_E \cos \lambda \cos(\phi_r + \Omega_r t)] \}, \end{aligned} \quad (58)$$

where  $\zeta = (h_o, \Phi_0, \alpha_1, \alpha_2, \omega_0, \dots, \omega_s)$ . Thus the signal (57) depends on  $5 + s$  parameters. We have computed the covariance matrices for this signal by means of Eqs. (52)–(54). The results are discussed below.

To study the dependence of the rms errors of the phase parameters on the observation time  $T_o$  we have considered a wide range of observation times from 1 hour to 4000 days. We have taken the latitude  $\lambda$  of the LIGO detector in Hanford and we have assumed the signal-to-noise ratio  $d = 10$ . We have considered five phase models given by Eq. (58) with  $s = 0, \dots, 4$  spindowns. The results of the numerical calculations are shown in Figure 10. We see that for observation times  $T_o$  up to  $\sim 20$  days the rms parameter errors decrease. For observation times from  $\sim 20$  days to  $\sim 100$  days the rms errors for initial phase  $\Phi_0$  and parameters  $\alpha_1$  and  $\alpha_2$  tend to decrease. The rate of the decrease is the smaller the more spindown parameters enter the phase of the signal and for higher spindown models the errors stay even constant for certain ranges of the observation time, whereas the frequency and the spindown errors in these ranges tend to increase. For high spindowns there is a range of observation time for which rms errors stay constant. For observation times from  $\sim 100$  days to  $\sim 1000$  days all the rms errors decrease and for observation times greater than  $\sim 1000$  days the rms errors level out to constant values. We have verified that all these constant values are to a very good accuracy equal to the rms errors of the polynomial phase model for the corresponding number of spindown parameters (these constant values can be found in Table 4 of Appendix C). Thus for observation times of more than  $\sim 3$  years the effect of the motion of the detector relative to the SSB has negligible effect for the rms errors of the initial phase, the frequency, and the spindown parameters.

The dependence of the rms phase parameters errors on the phase  $\phi_r$  which is determined by the initial position of the Earth in its diurnal motion is small. The errors vary by no more than  $\sim 10\%$  for the observation time  $T_o = 7$  days and for the phase models (58) with  $s = 0, \dots, 4$  spindowns (see Figure 11, where the model with  $s = 4$  spindowns is studied) assuming the signal-to-noise ratio  $d = 10$ . This dependence weakens when the observation time  $T_o$  increases.

The variations of the rms errors of the phase parameters with the initial phase  $\phi_o$  of the Earth's orbital motion are larger and depend in a complicated way on the observation time  $T_o$  and the number  $s$  of spindowns included in the phase model. For the observation time  $T_o = 120$  days and the phase model (58) with  $s = 4$  spindowns (assuming the signal-to-noise ratio  $d = 10$ ) the variations are less than  $\sim 10\%$  for all parameters except for parameters  $\alpha_1$  and  $\alpha_2$  where they are of order 100% (see Figure 12). For the observation time  $T_o = 120$  days and the signal-to-noise ratio  $d = 10$  the phase models (58) with  $s = 0, \dots, 3$  have the rms errors of all parameters that vary less with  $\phi_o$  compared to the  $s = 4$  model, with the exception of parameters  $\alpha_1$  and  $\alpha_2$ , for which the variations range from  $\sim 500\%$  to  $\sim 900\%$ . For the observation time  $T_o = 7$  days and the phase models (58) with  $s = 0, \dots, 4$  spindowns (assuming the signal-to-noise ratio  $d = 10$ ) the variations are less than  $\sim 10\%$  for all the parameters except again for the parameters  $\alpha_1$  and  $\alpha_2$ . For these parameters the variations range from  $\sim 10^{-7}\%$  for  $s = 4$  up to  $\sim 10^3\%$  for  $s = 0$ .

The rms errors of the phase parameters exhibit a sharp increase when the detector's location approaches the south or north pole. The dependence is weaker for the phase models (58) with smaller number  $s$  of spindowns included and it gets stronger when the observation time  $T_o$  increases. However the latitudes of the laser-interferometric detectors currently under construction range from 30.56 to 52.25 degrees (see Table I in Paper I) and in this interval the rms errors vary by no more than  $\sim 30\%$  for the observation time  $T_o = 120$  days and the phase model (58) with  $s = 4$  spindowns (see Figure 13) assuming the signal-to-noise ratio  $d = 10$ . The sharp increase of the rms errors when  $\lambda$  tends to  $\pm 90^\circ$  explains why the linear phase model II of Sec. 5.3 gives the errors significantly larger compared to another constant amplitude models (see Figures 8 and 9).

In Table 4 we have collected the rms errors of the initial phase  $\Phi_0$ , the parameters  $\alpha_1$ ,  $\alpha_2$ , and the spindowns  $f_o^{(k)}$  ( $k = 0, \dots, 4$ ) in the case of all-sky searches. We have considered five phase models (58) with  $s = 0, \dots, 4$  spindowns included and the observation times  $T_o$  of 7 and 120 days. The errors are calculated for the signal-to-noise ratio  $d = 10$  and they are inversely proportional to  $d$ . They are independent of the values of the spindown parameters in the signal. As a reference we quote the values of the spindowns for the Crab pulsar:  $f_o^{(1)} = -3.773 \times 10^{-10} \text{ s}^{-2}$ ,  $f_o^{(2)} = 0.976 \times 10^{-20} \text{ s}^{-3}$ , and  $f_o^{(3)} = -0.615 \times 10^{-30} \text{ s}^{-4}$ . We

see that in many cases the value of the rms error of a certain parameter does not change if we go from a model with  $k$  spindowns to a model with  $k + 1$  spindowns. For example for observation time of 7 days the rms error of frequency is almost the same for all the models. This merging of the errors is visible clearly in Figure 10 and occurs for certain ranges of the observation time. It is related to the merging for the polynomial phase model studied in Appendix C (see Figures 14 and 15).

The accuracy  $\Delta\Omega$  of the position of the source in the sky can be expressed in terms of the rms errors of  $\alpha_1$ ,  $\alpha_2$ , and  $f_o$  by means of the rule of propagation of errors.

We found in the previous section that for directed searches the polynomial phase model is adequate. Consequently in the case of directed searches we can completely neglect the dependence of the covariance matrices on the initial phases  $\phi_r$  and  $\phi_o$  and also on the latitude  $\lambda$  of the detector's location. The rms errors of the initial phase  $\Phi_0$  and the dimensionless spindown parameters  $\omega_k$  ( $k = 0, \dots, 4$ ) can be found in Table 4 of Appendix C. They are constant numbers, independent on the observation time  $T_o$ . However the rms errors of the spindown parameters  $f_o^{(k)}$  ( $k = 0, \dots, 4$ ) do depend on the observation time  $T_o$  and this dependence is described by Eq. (56).

In Table 5 we have given the rms errors of the initial phase  $\Phi_0$  and the spindowns  $f_o^{(k)}$  ( $k = 0, \dots, 4$ ) for directed searches. We have considered five polynomial phase models with  $s = 0, \dots, 4$  spindowns included and the observation times  $T_o$  of 7 and 120 days. The errors are calculated for the signal-to-noise ratio  $d = 10$  and they are inversely proportional to  $d$ .

The fact that in some cases (both in all-sky and directed searches) the errors of the parameters do not change when we go to a model with one more spindown is a result of a special choice of the initial time of the observation which was chosen to be in the middle of the observation interval. This effect is studied in detail in Appendix C (see Figure 14).

$s$	$\sigma(\Phi_0)$ (rad)	$\sigma(\alpha_1)$ (s <sup>-1</sup> )	$\sigma(\alpha_2)$ (s <sup>-1</sup> )	$\sigma(f_o)$ (s <sup>-1</sup> )	$\sigma(f_o^{(1)})$ (s <sup>-2</sup> )	$\sigma(f_o^{(2)})$ (s <sup>-3</sup> )	$\sigma(f_o^{(3)})$ (s <sup>-4</sup> )	$\sigma(f_o^{(4)})$ (s <sup>-5</sup> )
$T_o = 7$ days								
0	$1.8 \times 10^2$	1.6	0.21	$1.6 \times 10^{-4}$				
1	$4.9 \times 10^3$	1.6	1.6	$1.6 \times 10^{-4}$	$3.1 \times 10^{-11}$			
2	$4.9 \times 10^3$	1.7	1.6	$1.7 \times 10^{-4}$	$3.1 \times 10^{-11}$	$2.4 \times 10^{-17}$		
3	$4.9 \times 10^3$	1.7	1.6	$1.7 \times 10^{-4}$	$3.1 \times 10^{-11}$	$2.4 \times 10^{-17}$	$6.0 \times 10^{-22}$	
4	$5.0 \times 10^3$	1.7	1.6	$1.7 \times 10^{-4}$	$3.2 \times 10^{-11}$	$1.0 \times 10^{-16}$	$6.0 \times 10^{-22}$	$2.0 \times 10^{-26}$
$T_o = 120$ days								
0	0.57	$1.2 \times 10^{-3}$	$2.6 \times 10^{-4}$	$1.1 \times 10^{-7}$				
1	29	$1.7 \times 10^{-3}$	$9.2 \times 10^{-3}$	$1.1 \times 10^{-7}$	$1.7 \times 10^{-13}$			
2	29	$8.8 \times 10^{-2}$	$1.4 \times 10^{-2}$	$8.8 \times 10^{-6}$	$1.7 \times 10^{-13}$	$3.3 \times 10^{-19}$		
3	$2.7 \times 10^3$	0.14	0.85	$8.8 \times 10^{-6}$	$1.7 \times 10^{-11}$	$3.3 \times 10^{-19}$	$6.4 \times 10^{-25}$	
4	$2.7 \times 10^3$	1.7	0.87	$1.6 \times 10^{-4}$	$1.7 \times 10^{-11}$	$6.5 \times 10^{-18}$	$6.4 \times 10^{-25}$	$2.5 \times 10^{-31}$

Table 4: The rms errors of the initial phase  $\Phi_0$ , the parameters  $\alpha_1$ ,  $\alpha_2$ , and the spindowns  $f_o^{(k)}$  ( $k = 0, \dots, 4$ ) for all-sky searches. We have approximated the gravitational-wave signal by the one-component constant amplitude and linear phase model of Sec. 5.2. We have considered five phase models with  $s = 0, \dots, 4$  spindowns included and the observation times  $T_o$  of 7 and 120 days. The signal-to-noise ratio  $d = 10$ . We have assumed the latitude  $\lambda$  of the Hanford LIGO detector, we have also put  $\phi_r = 1.456$  and  $\phi_o = 0.123$ .

## Acknowledgments

We would like to thank the Albert Einstein Institute, Max Planck Institute for Gravitational Physics for hospitality. We would also like to thank Bernard F. Schutz for many useful discussions, comments, and suggestions that led to a considerable improvement of this work. This work was supported in part by Polish Science Committee grant KBN 2 P303D 021 11.

$s$	$\sigma(\Phi_0)$ (rad)	$\sigma(f_o)$ (s <sup>-1</sup> )	$\sigma(f_o^{(1)})$ (s <sup>-2</sup> )	$\sigma(f_o^{(2)})$ (s <sup>-3</sup> )	$\sigma(f_o^{(3)})$ (s <sup>-4</sup> )	$\sigma(f_o^{(4)})$ (s <sup>-5</sup> )
$T_o = 7$ days						
0	0.10	$9.1 \times 10^{-8}$				
1	0.15	$9.1 \times 10^{-8}$	$1.2 \times 10^{-12}$			
2	0.15	$2.3 \times 10^{-7}$	$1.2 \times 10^{-12}$	$2.3 \times 10^{-17}$		
3	0.19	$2.3 \times 10^{-7}$	$4.1 \times 10^{-12}$	$2.3 \times 10^{-17}$	$6.0 \times 10^{-22}$	
4	0.19	$4.0 \times 10^{-7}$	$4.1 \times 10^{-12}$	$1.0 \times 10^{-16}$	$6.0 \times 10^{-22}$	$2.0 \times 10^{-26}$
$T_o = 120$ days						
0	0.10	$5.3 \times 10^{-9}$				
1	0.15	$5.3 \times 10^{-9}$	$4.0 \times 10^{-15}$			
2	0.15	$1.3 \times 10^{-8}$	$4.0 \times 10^{-15}$	$4.5 \times 10^{-21}$		
3	0.19	$1.3 \times 10^{-8}$	$1.4 \times 10^{-14}$	$4.5 \times 10^{-21}$	$6.9 \times 10^{-27}$	
4	0.19	$2.3 \times 10^{-8}$	$1.4 \times 10^{-14}$	$2.0 \times 10^{-20}$	$6.9 \times 10^{-27}$	$1.3 \times 10^{-32}$

Table 5: The rms errors of the initial phase  $\Phi_0$  and the spindowns  $f_o^{(k)}$  ( $k = 0, \dots, 4$ ) for directed searches. We have approximated the gravitational-wave signal by the one-component constant amplitude and polynomial phase model of Sec. 5.4. We have considered five phase models with  $s = 0, \dots, 4$  spindowns included and the observation times  $T_o$  of 7 and 120 days. We have assumed the signal-to-noise ratio  $d = 10$ .

## A 1/4 of a cycle criterion

The fitting factor FF between a signal  $h = h(t; \boldsymbol{\theta})$  and a filter  $h' = h'(t; \boldsymbol{\theta}')$  ( $\boldsymbol{\theta}$  and  $\boldsymbol{\theta}'$  are the parameters of the signal and the filter, respectively) is defined as [13]

$$\text{FF} := \max_{\boldsymbol{\theta}'} \frac{(h(t; \boldsymbol{\theta}) | h'(t; \boldsymbol{\theta}'))}{\sqrt{(h(t; \boldsymbol{\theta}) | h(t; \boldsymbol{\theta}))} \sqrt{(h'(t; \boldsymbol{\theta}') | h'(t; \boldsymbol{\theta}'))}}. \quad (59)$$

$1 - \text{FF}$  gives the fraction of the signal-to-noise lost when using a filter not perfectly matched to a signal. For narrowband signals around the frequency  $f_o$  the scalar product  $(\cdot | \cdot)$  can be computed from the formula

$$(h_1 | h_2) \cong \frac{2}{S_h(f_o)} \int_{-T_o/2}^{T_o/2} h_1(t) h_2(t) dt, \quad (60)$$

where  $S_h$  is the one-sided noise spectral density and  $T_o$  is the observation time.

Let us assume that the signal and the filter can be written as

$$h(t; \boldsymbol{\theta}) = h_o \sin \Psi(t; \boldsymbol{\zeta}), \quad (61)$$

$$h'(t; \boldsymbol{\theta}') = h'_o \sin \Psi'(t; \boldsymbol{\zeta}'), \quad (62)$$

where  $h_o$  and  $h'_o$  are constant amplitudes,  $\boldsymbol{\zeta}$  and  $\boldsymbol{\zeta}'$  denote the parameters entering the phases  $\Psi$  and  $\Psi'$  of the signal and the filter, respectively. We substitute Eqs. (61) and (62) into Eq. (59). Using Eq. (60) we obtain

$$\text{FF} \cong \max_{\boldsymbol{\zeta}'} \frac{1}{T_o} \int_{-T_o/2}^{T_o/2} \cos [\Psi(t; \boldsymbol{\zeta}) - \Psi'(t; \boldsymbol{\zeta}')] dt. \quad (63)$$

The fitting factor attains its maximum value of 1 when the functions  $\Psi$  and  $\Psi'$  are the same and when values of the parameters in the signal and the filter coincide. When  $\Psi$  and  $\Psi'$  are not the same because in the phase of the filter we have not taken into account some effects present in the signal the fitting factor is less than 1. Moreover the values of the parameter in the filter that maximize the correlation integral will be biased, i.e. shifted away from the true values in the signal.

For the simplest nontrivial case of the difference between the phase of the filter and the phase of the signal consisting of a constant phase  $\phi$  and a term linear in time (with a constant frequency  $f$ ) the fitting factor (63) equals

$$\text{FF} \cong \max_{\phi} \frac{1}{T_o} \int_{-T_o/2}^{T_o/2} \cos(2\pi ft + \phi) dt. \quad (64)$$

We easily get

$$\text{FF} \cong \max_{\phi} \left[ \frac{\sin(\pi f T_o)}{\pi f T_o} \cos \phi \right] = \frac{\sin(\pi f T_o)}{\pi f T_o}. \quad (65)$$

If the frequency  $f$  is such that it produces not more than  $1/4$  of a cycle during the observation time  $T_o$  (i.e.  $fT_o \leq 1/4$ ) then from Eq. (65) we obtain

$$\text{FF} \gtrsim \frac{\sin \frac{\pi}{4}}{\frac{\pi}{4}} \cong 0.900.$$

Thus characterization of the  $1/4$  of a cycle criterion is the following: *for the simplest nontrivial case discarding a term in the phase that contributes less than  $1/4$  of a cycle over observation time leads to a loss in signal-to-noise ratio of not more than 10%.*

## B Number of cycles

The model of the phase of the signal at the detector given by Eq. (12) can be rewritten as

$$\Psi = \Phi_0 + 2\pi \sum_{k=0}^{s_1} N_k + 2\pi \sum_{k=0}^{s_2} N_k^{(o)} + 2\pi \sum_{k=0}^{s_3} N_k^{(r)}, \quad (66)$$

where  $N_k$ ,  $N_k^{(o)}$  and  $N_k^{(r)}$  denote the numbers of cycles arising from the term polynomial in time, the orbital motion and the rotational motion of the detector, respectively:

$$N_k := f_g^{(k)} \frac{t^{k+1}}{(k+1)!}, \quad N_k^{(o)} := f_g^{(k)} \frac{t^k}{k!} \frac{\mathbf{n}_0 \cdot \mathbf{r}_{ES}}{c}, \quad N_k^{(r)} := f_g^{(k)} \frac{t^k}{k!} \frac{\mathbf{n}_0 \cdot \mathbf{r}_E}{c}, \quad (67)$$

where  $f_g$  and  $f_g^{(k)}$  are respectively the frequency and the spindown parameters of the gravitational-wave signal. The moduli of the quantities  $N_k$ ,  $N_k^{(o)}$  and  $N_k^{(r)}$  can be estimated as follows:

$$|N_k| = \bar{N}_k := \left| f_g^{(k)} \right| \frac{t^{k+1}}{(k+1)!}, \quad (68)$$

$$\left| N_k^{(o)} \right| \leq \bar{N}_k^{(o)} := \left| f_g^{(k)} \right| \frac{t^k}{k!} \frac{r_{ES}}{c}, \quad \left| N_k^{(r)} \right| \leq \bar{N}_k^{(r)} := \left| f_g^{(k)} \right| \frac{t^k}{k!} \frac{r_E}{c}. \quad (69)$$

We estimate the maximum values of the spindown parameters  $f_g^{(k)}$  from the following formula

$$\left| f_g^{(k)} \right| \simeq k! \frac{f_g}{\tau^k}, \quad (70)$$

where  $\tau$  is the spindown age of the neutron star. Using Eq. (70) the quantities  $\bar{N}_k$ ,  $\bar{N}_k^{(o)}$  and  $\bar{N}_k^{(r)}$  can be estimated as follows:

$$\bar{N}_k \simeq f_g t \frac{1}{k+1} \left( \frac{t}{\tau} \right)^k, \quad (71)$$

$$\bar{N}_k^{(o)} \simeq f_g \frac{r_{ES}}{c} \left( \frac{t}{\tau} \right)^k, \quad \bar{N}_k^{(r)} \simeq f_g \frac{r_E}{c} \left( \frac{t}{\tau} \right)^k. \quad (72)$$

Let us note that the ratios of the different contributions for the fixed  $k$  do not depend on the gravitational-wave frequency  $f_g$  and the spindown age  $\tau$ :

$$\frac{\bar{N}_k^{(r)}}{\bar{N}_k} \simeq (k+1) \frac{r_E}{ct}, \quad \frac{\bar{N}_k^{(o)}}{\bar{N}_k} \simeq (k+1) \frac{r_{ES}}{ct}. \quad (73)$$

From the formulae given above it is easy to obtain how many terms are needed in each of the three series on the right-hand side of Eq. (12) for the eight models of the phase considered in our simulations in order to meet the criterion that all terms that contribute more than  $1/4$  of a cycle are included. The results are summarized in Table 1 of Sec. 2.

## C Polynomial phase model

The ability to control the values of the Fisher information matrix for the frequency of the signal and its derivatives may be useful in real data processing schemes. Therefore in this appendix we study the



dependence of the Fisher matrix on the choice of the instant of time at which the instantaneous frequency and spindown parameters are defined.

We use the one-component signal with a constant amplitude and the phase polynomial in time, which is introduced in Sec. 5.4. Such a signal can be written as

$$h(t; h_o, \zeta) = h_o \sin \Psi(t; \zeta), \quad (74)$$

where  $h_o$  is a constant amplitude and  $\zeta$  denotes the parameters entering the phase  $\Psi$  of the signal. As the signal (74) has the constant amplitude, the formulae (46)–(54) from Sec. 6 can be applied here. But here unlike in Sec. 6 we choose the observation interval to be  $[0, T_o]$ , where  $T_o$  is the observation time. We also introduce the dimensionless variable  $x := t/T_o$ . Then the formulae (52)–(54) for the components of the covariance matrix  $C$  can be rewritten as

$$C_{h_o h_o} \cong \frac{h_o^2}{d^2}, \quad (75)$$

$$C_{h_o \zeta_i} \cong 0, \quad (76)$$

$$C_{\zeta_i \zeta_j} \cong \frac{1}{d^2} \left( \tilde{\Gamma}^{-1} \right)_{\zeta_i \zeta_j}, \quad (77)$$

where the optimal signal-to-noise ratio  $d$  is given by Eq. (46) and the reduced Fisher matrix  $\tilde{\Gamma}$  is defined by

$$\tilde{\Gamma}_{\zeta_i \zeta_j} := \int_0^1 \frac{\partial \Psi}{\partial \zeta_i} \frac{\partial \Psi}{\partial \zeta_j} dx. \quad (78)$$

Using the dimensionless variable  $x$  the polynomial phase is defined as

$$\Psi(x; \zeta) = \Phi_0 + \sum_{k=0}^s \omega_k (x - x_0)^{k+1}, \quad (79)$$

where  $x_0$  is an arbitrarily chosen initial time,  $\Phi_0$  denotes the initial phase, and  $\omega_k$  ( $k = 0, \dots, s$ ) are the spindown parameters, so  $\zeta = (\Phi_0, \omega_0, \dots, \omega_s)$ .

The reduced Fisher matrix  $\tilde{\Gamma}$  for the polynomial phase model (79) has the structure very similar to that of the  $(s + 2)$ -dimensional Hilbert matrix. For  $x_0 = 0$   $\tilde{\Gamma}$  is the  $(s + 2)$ -dimensional Hilbert matrix. For  $s = 4$  (four spindown parameters included) the reduced Fisher matrix  $\tilde{\Gamma}$  computed for an arbitrary  $x_0$  equals

$$\tilde{\Gamma} = \begin{pmatrix} \Gamma_1 & \Gamma_2 & \Gamma_3 & \Gamma_4 & \Gamma_5 & \Gamma_6 \\ & \Gamma_3 & \Gamma_4 & \Gamma_5 & \Gamma_6 & \Gamma_7 \\ & & \Gamma_5 & \Gamma_6 & \Gamma_7 & \Gamma_8 \\ & & & \Gamma_7 & \Gamma_8 & \Gamma_9 \\ & & & & \Gamma_9 & \Gamma_{10} \\ & & & & & \Gamma_{11} \end{pmatrix}, \quad (80)$$

where

$$\begin{aligned} \Gamma_1 &= 1, \\ \Gamma_2 &= 1/2 - x_0, \\ \Gamma_3 &= 1/3 - x_0 + x_0^2, \\ \Gamma_4 &= (1 - 4x_0 + 6x_0^2 - 4x_0^3)/4, \\ \Gamma_5 &= 1/5 - x_0 + 2x_0^2 - 2x_0^3 + x_0^4, \\ \Gamma_6 &= (1 - 6x_0 + 15x_0^2 - 20x_0^3 + 15x_0^4 - 6x_0^5)/6, \\ \Gamma_7 &= 1/7 - x_0 + 3x_0^2 - 5x_0^3 + 5x_0^4 - 3x_0^5 + x_0^6, \\ \Gamma_8 &= 1/8 - x_0 + (7x_0^2)/2 - 7x_0^3 + (35x_0^4)/4 - 7x_0^5 + (7x_0^6)/2 - x_0^7, \\ \Gamma_9 &= 1/9 - x_0 + 4x_0^2 - (28x_0^3)/3 + 14x_0^4 - 14x_0^5 + (28x_0^6)/3 - 4x_0^7 + x_0^8, \\ \Gamma_{10} &= 1/10 - x_0 + (9x_0^2)/2 - 12x_0^3 + 21x_0^4 - (126x_0^5)/5 + 21x_0^6 - 12x_0^7 + (9x_0^8)/2 - x_0^9, \\ \Gamma_{11} &= 1/11 - x_0 + 5x_0^2 - 15x_0^3 + 30x_0^4 - 42x_0^5 + 42x_0^6 - 30x_0^7 + 15x_0^8 - 5x_0^9 + x_0^{10}. \end{aligned}$$

After putting  $x_0 = 0$  into the above formulae one obtains the 6-dimensional Hilbert matrix:

$$\tilde{\Gamma} = \begin{pmatrix} 1 & 1/2 & 1/3 & 1/4 & 1/5 & 1/6 \\ 1/2 & 1/3 & 1/4 & 1/5 & 1/6 & 1/7 \\ 1/3 & 1/4 & 1/5 & 1/6 & 1/7 & 1/8 \\ 1/4 & 1/5 & 1/6 & 1/7 & 1/8 & 1/9 \\ 1/5 & 1/6 & 1/7 & 1/8 & 1/9 & 1/10 \\ 1/6 & 1/7 & 1/8 & 1/9 & 1/10 & 1/11 \end{pmatrix}. \quad (81)$$

$s$	$\sigma(\Phi_0)d$	$\sigma(\omega_0)d$	$\sigma(\omega_1)d$	$\sigma(\omega_2)d$	$\sigma(\omega_3)d$	$\sigma(\omega_4)d$
0	1	$2\sqrt{3}$				
1	3/2	$2\sqrt{3}$	$6\sqrt{5}$			
2	3/2	$5\sqrt{3}$	$6\sqrt{5}$	$20\sqrt{7}$		
3	15/8	$5\sqrt{3}$	$21\sqrt{5}$	$20\sqrt{7}$	210	
4	15/8	$35\sqrt{3}/4$	$21\sqrt{5}$	$90\sqrt{7}$	210	$252\sqrt{11}$

Table 6: The rms errors  $\sigma(\zeta_k)$  of the phase parameters  $\zeta = (\Phi_0, \omega_0, \dots, \omega_4)$  for the polynomial models with  $s = 0, \dots, 4$  spindowns. We have assumed the initial time  $x_0 = 0.5$ .

We have computed the rms errors of the phase parameters  $\zeta_k$  for five different phase models (79) with  $s = 0, \dots, 4$ . The rms errors  $\sigma(\zeta_k)$  are the square roots of the diagonal elements of the reduced covariance matrices  $\tilde{C} = \tilde{\Gamma}^{-1}$ . In Figure 14 the errors  $\sigma(\zeta_k)$  are plotted as functions of the initial time  $x_0$ . It is seen from the figure that the errors depend on the choice of the initial time  $x_0$ . This can be explained as follows. The phase  $\Psi$  of the signal at a given time  $x$  does not depend on the choice of the initial time  $x_0$ . Thus for the two different choices  $x_{01}$  and  $x_{02}$  of the initial time  $x_0$  we have

$$\Phi_{01} + \sum_{k=0}^s \omega_{k1}(x - x_{01})^{k+1} = \Phi_{02} + \sum_{k=0}^s \omega_{k2}(x - x_{02})^{k+1}, \quad (82)$$

where the parameters  $\Phi_{01}, \omega_{k1}$  and  $\Phi_{02}, \omega_{k2}$  are associated with the initial times  $x_{01}$  and  $x_{02}$ , respectively. Using Eq. (82) one can, for fixed  $s$ , express the parameters  $\zeta_1 = (\Phi_{01}, \omega_{01}, \dots, \omega_{s1})$  as linear combinations of  $\zeta_2 = (\Phi_{02}, \omega_{02}, \dots, \omega_{s2})$ :

$$\zeta_{2l} = \sum_{n=0}^{s+2} j_{ln}(x_{01}, x_{02}) \zeta_{1n}, \quad (83)$$

where  $j_{ln}$  are the components of the transformation matrix  $J$  given by

$$J = \begin{pmatrix} 1 & x_{02} - x_{01} & (x_{02} - x_{01})^2 & (x_{02} - x_{01})^3 & (x_{02} - x_{01})^4 & (x_{02} - x_{01})^5 \\ 0 & 1 & 2(x_{02} - x_{01}) & 3(x_{02} - x_{01})^2 & 4(x_{02} - x_{01})^3 & 5(x_{02} - x_{01})^4 \\ 0 & 0 & 1 & 3(x_{02} - x_{01}) & 6(x_{02} - x_{01})^2 & 10(x_{02} - x_{01})^3 \\ 0 & 0 & 0 & 1 & 4(x_{02} - x_{01}) & 10(x_{02} - x_{01})^2 \\ 0 & 0 & 0 & 0 & 1 & 5(x_{02} - x_{01}) \\ 0 & 0 & 0 & 0 & 0 & 1 \end{pmatrix}. \quad (84)$$

Thus the change of the initial time from  $x_{01}$  to  $x_{02}$  corresponds to estimating a different set of parameters given by a linear combination of the original parameters. For example the new frequency parameter defined as the first derivative of the phase at time  $x_{02}$  (divided by  $2\pi$ ) is a linear combination of the frequency parameter and spindown parameters at time  $x_{01}$ . Let us denote by  $C(x_{01})$  and  $C(x_{02})$  the covariance matrices for the parameters  $\zeta_{1l}$  and  $\zeta_{2l}$ , respectively. It is easy to see that these matrices are related by

$$C(x_{02}) = JC(x_{01})J^T. \quad (85)$$

The dependence of the rms errors of the signal parameters on the choice of the initial time for the full phase model is very similar to that observed in the polynomial model considered above. This is illustrated in Figure 15, where we have plotted the simulated cumulative distribution functions of the parameter errors for the full model of the signal described in Sec. 2. The initial time  $t_o = 0$  used in the simulations coincides with the middle of the observation interval which is  $[-T_o/2, T_o/2]$ , so it corresponds to  $x_0 = 0.5$ . The comparison of Figures 14 and 15 shows that the curve merging observed in Figure 15 exactly corresponds to intersection points observed in Figure 14 for  $x_0 = 0.5$ .

Finally in Table 6 we give the rms errors (diagonal components of the inverse of the Fisher matrix) of the parameters  $\zeta$  in various polynomial models. We consider models with  $s = 0, \dots, 4$  spindowns and we assume  $x_0 = 0.5$ .

## References

- [1] K. Danzmann *et al.*, in *Gravitational Wave Experiments*, edited by E. Coccia, G. Pizzella, and F. Ronga (World Scientific, Singapore, 1995), pp. 100–111.
- [2] A. Abramovici *et al.*, *Science* **256**, 325 (1992).

- [3] C. Bradaschia *et al.*, Nucl. Instrum. Methods Phys. Res. A **289**, 518 (1990).
- [4] K. Tsubono *et al.*, in *Gravitational Wave Detection. Proceedings of the TAMA International Workshop on Gravitational Wave Detection*, edited by K. Tsubono, M.-K. Fujimoto, and K. Kuroda (Universal Academy Press, Tokyo, 1997), pp. 183–191.
- [5] P. Jaranowski, A. Królak, and B. F. Schutz, Phys. Rev. D **58**, 063001 (1998).
- [6] P. R. Brady, T. Creighton, C. Cutler, and B. F. Schutz, Phys. Rev. D **57**, 2101 (1998).
- [7] B. F. Schutz, Class. Quantum Grav. **13**, A219 (1996).
- [8] S. Kawamura (private communication).
- [9] K. Strain (private communication).
- [10] Quantile  $q_x$  gives a value  $z_x$  of random variable  $z$  such that probability that  $z < z_x$  is less than or equal to  $x$ . The quantile values at  $x = 0.25, 0.5$ , and  $0.75$  are called the quartiles.
- [11] D. R. Lorimer, M. Bailes, and P. A. Harrison, Mon. Not. R. Astron. Soc. **289**, 592 (1997).
- [12] J. H. Taylor, R. N. Manchester, A. G. Lyne, and F. Camilo, Catalog of 706 pulsars (1995).
- [13] T. A. Apostolatos, Phys. Rev. D **52**, 605 (1995).
- [14] A. Królak, K. D. Kokkotas, and G. Schäfer, Phys. Rev. D **52**, 2089 (1995).
- [15] A. Królak, in *Very High Energy Phenomena in the Universe. Proceedings of the XXXII<sup>nd</sup> Rencontres de Moriond*, edited by Y. Giraud-Héraud and J. Trân Thanh Vân (Editions Frontieres, Paris, 1997), pp. 329–334.

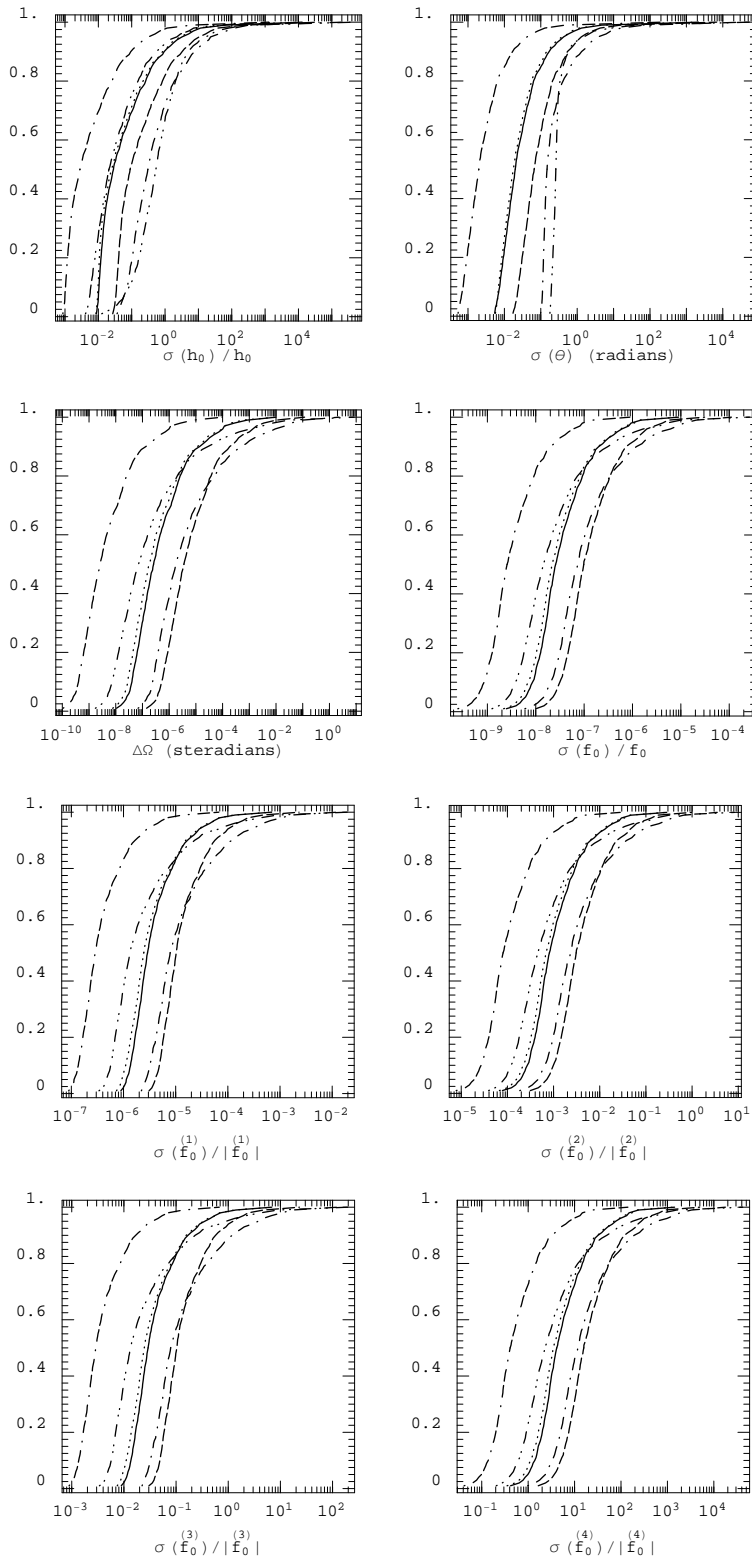


Figure 1: Cumulative distribution functions of the simulated rms errors of the signal parameters for the individual detectors in the case of all-sky searches. The observation time  $T_o = 120$  days. We assume that star's ellipticity  $\epsilon = 10^{-5}$ , its moment of inertia w.r.t. the rotation axis  $I = 10^{45}$  g cm<sup>2</sup>, its distance from the Earth  $r_o = 1$  kpc, and the frequency  $f_o = 500$  Hz [these values give the dimensionless amplitude of the waveform  $h_o = 1.1 \times 10^{-23}$ , cf. Eq. (5)]. The spindown age  $\tau = 40$  years. The model of the signal's phase is described by  $s_1 = 4$ ,  $s_2 = 3$ , and  $s_3 = 0$  (cf. Table 1). The lines given on the diagrams correspond to various detectors: advanced Hanford (dotted/double dashed), initial Hanford (solid), VIRGO (dotted), wideband GEO600 (dashed), narrowband GEO600 (double dotted/dashed), and TAMA300 (dotted/dashed). On the left top panel we have also put the extra double dotted/double dashed curve. It describes cumulative distribution function of the relative rms error of the amplitude  $h'_o = h_o \sin^2 \theta$  of the second component of the signal as measured by the GEO600 narrowband detector.

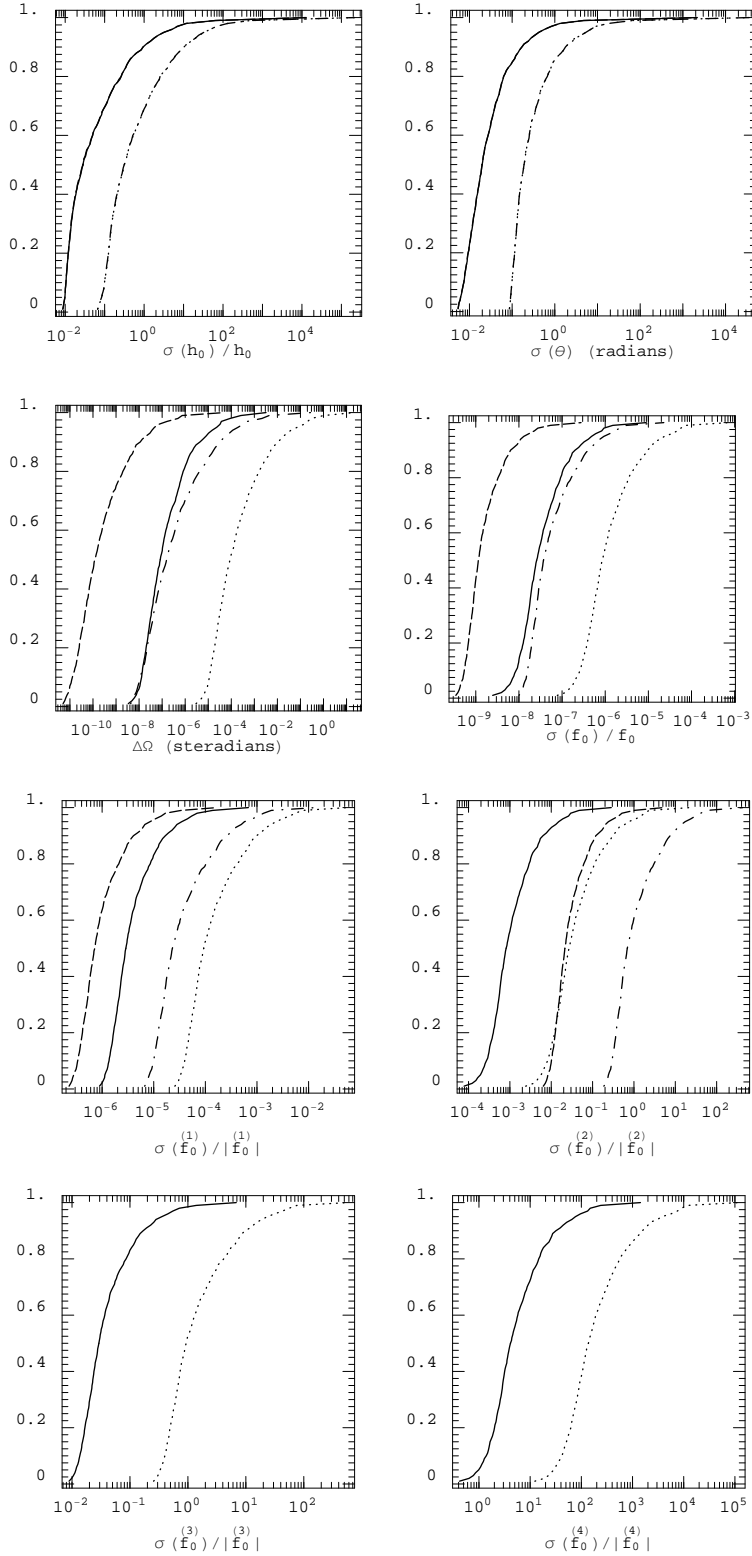


Figure 2: Cumulative distribution functions of the simulated rms errors of the signal parameters for various models of the signal in the case of all-sky searches. The observation time  $T_o = 120$  days. The initial Hanford detector is assumed in the simulations. The neutron star parameters are the same as in Figure 1. The lines shown in the diagrams correspond to the following models of the signal:  $f_o = 500$  Hz,  $\tau = 40$  yr,  $s_1 = 4$ ,  $s_2 = 3$ ,  $s_3 = 0$  (solid),  $f_o = 500$  Hz,  $\tau = 1000$  yr,  $s_1 = 2$ ,  $s_2 = 1$ ,  $s_3 = 0$  (dashed),  $f_o = 100$  Hz,  $\tau = 40$  yr,  $s_1 = 4$ ,  $s_2 = 2$ ,  $s_3 = 0$  (dotted),  $f_o = 100$  Hz,  $\tau = 1000$  yr,  $s_1 = 2$ ,  $s_2 = 1$ ,  $s_3 = 0$  (dotted/dashed). The dimensionless amplitude of the waveform  $h_o = 1.1 \times 10^{-23}$  for the models with  $f_o = 500$  Hz and  $h_o = 4.2 \times 10^{-25}$  for the models with  $f_o = 100$  Hz. On the two top panels the lines which correspond to the models with the same frequency  $f_o$  coincide.

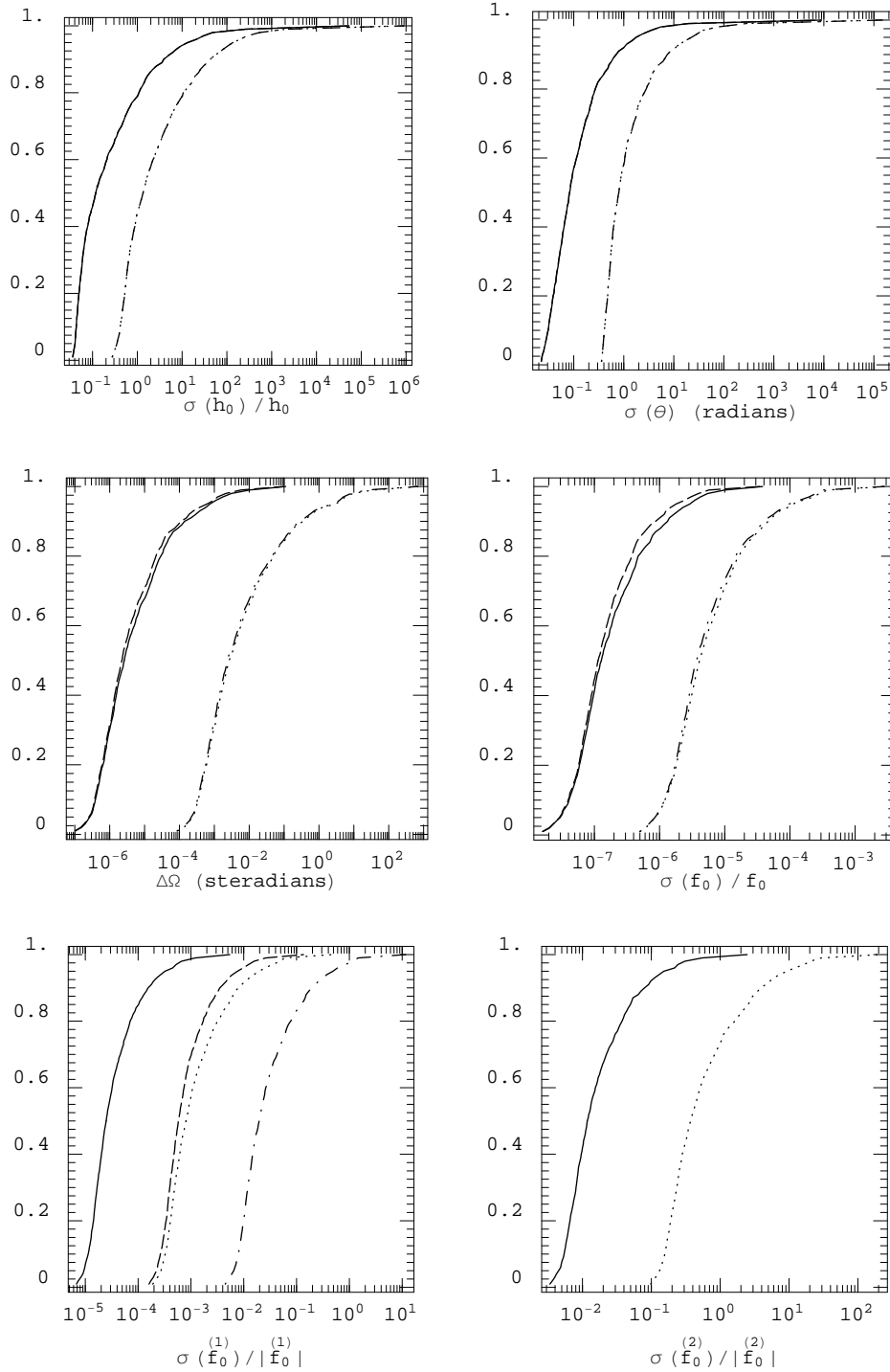


Figure 3: Cumulative distribution functions of the simulated rms errors of the signal parameters for various models of the signal in the case of all-sky searches. The observation time  $T_o = 7$  days. The initial Hanford detector is assumed in the simulations. The neutron star parameters are the same as in Figure 1. The lines shown in the diagrams correspond to the following models of the signal:  $f_o = 500$  Hz,  $\tau = 40$  yr,  $s_1 = 2$ ,  $s_2 = 1$ ,  $s_3 = 0$  (solid),  $f_o = 500$  Hz,  $\tau = 1000$  yr,  $s_1 = 1$ ,  $s_2 = 1$ ,  $s_3 = 0$  (dashed),  $f_o = 100$  Hz,  $\tau = 40$  yr,  $s_1 = 2$ ,  $s_2 = 1$ ,  $s_3 = 0$  (dotted),  $f_o = 100$  Hz,  $\tau = 1000$  yr,  $s_1 = 1$ ,  $s_2 = 1$ ,  $s_3 = 0$  (dotted/dashed). The dimensionless amplitude of the waveform  $h_o = 1.1 \times 10^{-23}$  for the models with  $f_o = 500$  Hz and  $h_o = 4.2 \times 10^{-25}$  for the models with  $f_o = 100$  Hz. On the two top panels the lines which correspond to the models with the same frequency  $f_o$  coincide.

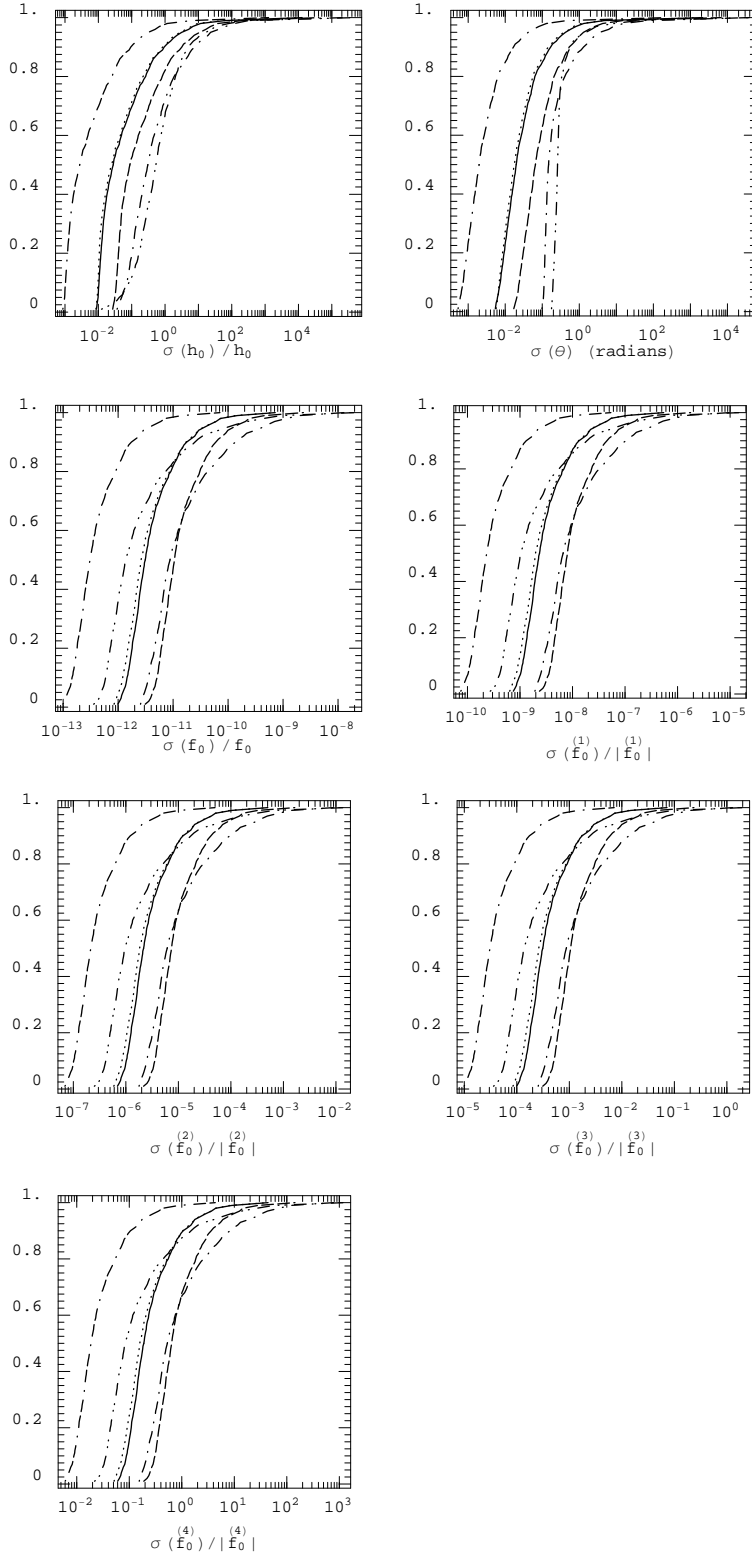


Figure 4: Cumulative distribution functions of the simulated rms errors of the signal parameters for the individual detectors in the case of directed searches. The observation time  $T_o = 120$  days. The neutron star parameters are the same as in Figure 1. The model of the signal's phase is described by  $s_1 = 4$ ,  $s_2 = 3$ , and  $s_3 = 0$ . The lines given on the diagrams correspond to various detectors: advanced Hanford (dotted/double dashed), initial Hanford (solid), VIRGO (dotted), wideband GEO600 (dashed), narrowband GEO600 (double dotted/dashed), and TAMA300 (dotted/dashed).

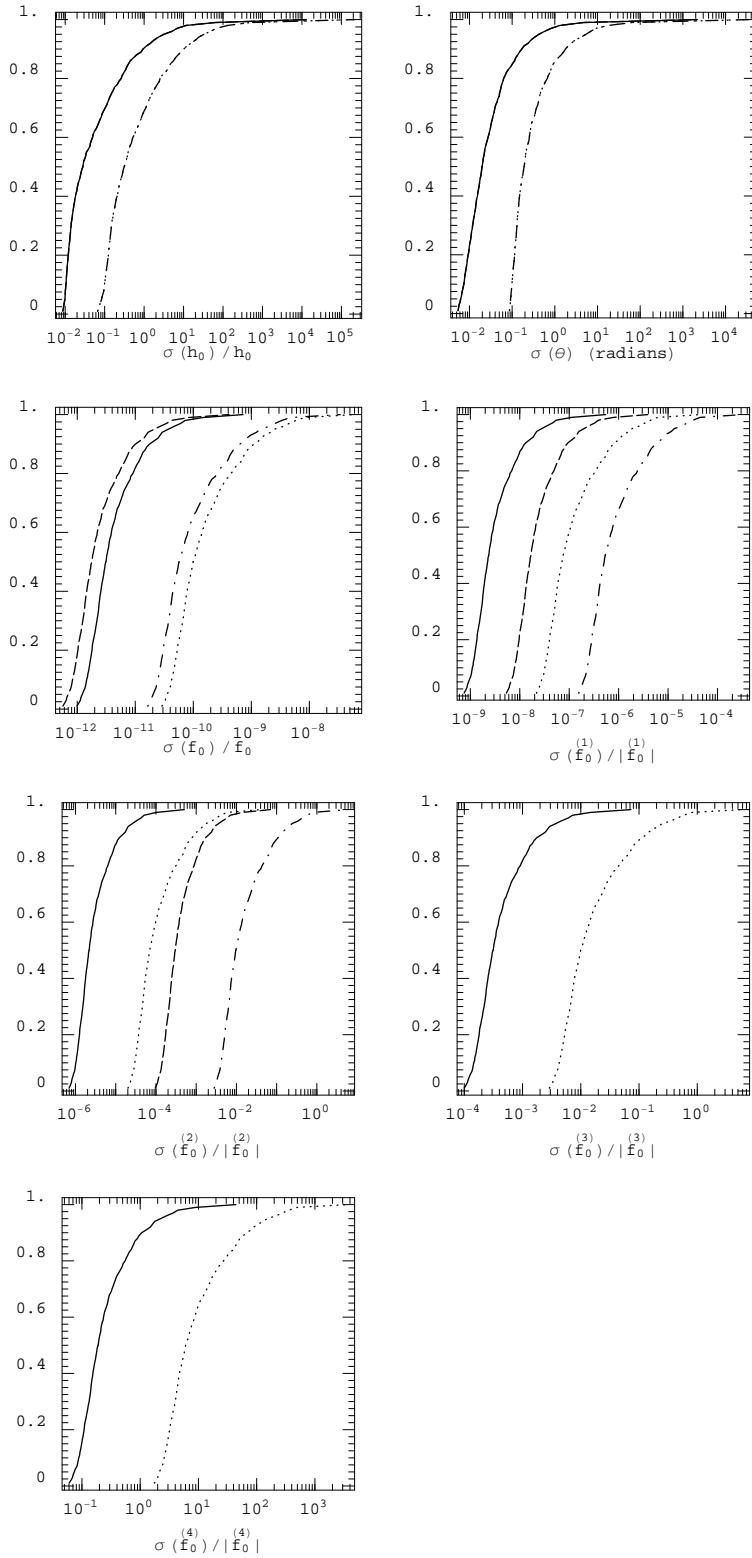


Figure 5: Cumulative distribution functions of the simulated rms errors of the signal parameters for directed searches and various models of the signal. The observation time  $T_o = 120$  days. The initial Hanford detector is assumed in the simulations. The neutron star parameters are the same as in Figure 1. The lines shown in the diagrams correspond to the following models of the parameter space:  $f_o = 500$  Hz,  $\tau = 40$  yr,  $s_1 = 4$ ,  $s_2 = 3$ ,  $s_3 = 0$  (solid),  $f_o = 500$  Hz,  $\tau = 1000$  yr,  $s_1 = 2$ ,  $s_2 = 1$ ,  $s_3 = 0$  (dashed),  $f_o = 100$  Hz,  $\tau = 40$  yr,  $s_1 = 4$ ,  $s_2 = 2$ ,  $s_3 = 0$  (dotted),  $f_o = 100$  Hz,  $\tau = 1000$  yr,  $s_1 = 2$ ,  $s_2 = 1$ ,  $s_3 = 0$  (dotted/dashed). The dimensionless amplitude of the waveform  $h_o = 1.1 \times 10^{-23}$  for the models with  $f_o = 500$  Hz and  $h_o = 4.2 \times 10^{-25}$  for the models with  $f_o = 100$  Hz. On the two top panels the lines which correspond to the models with the same frequency  $f_o$  coincide.



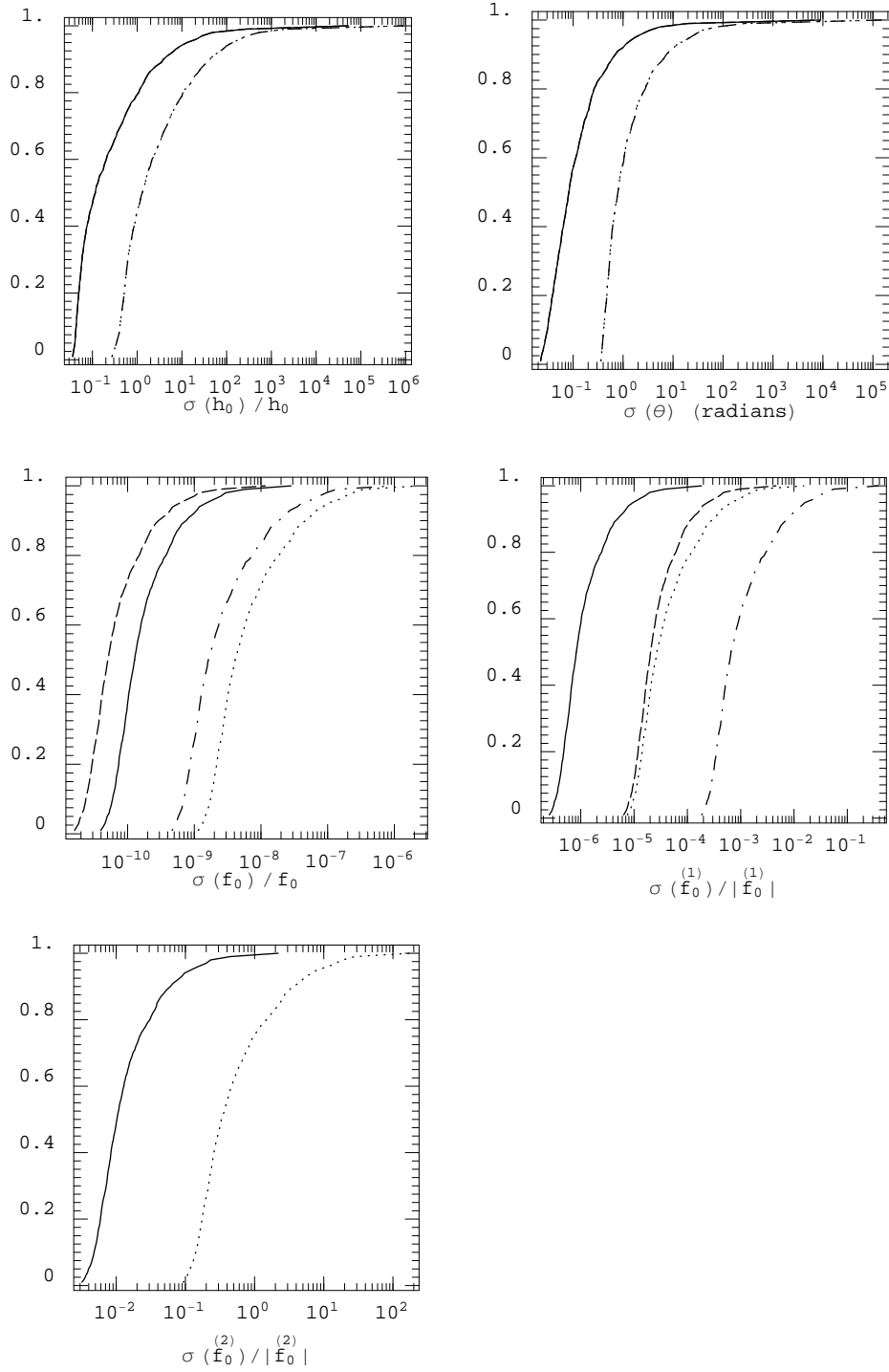


Figure 6: Cumulative distribution functions of the simulated rms errors of the signal parameters for directed searches and various models of the signal. The observation time  $T_o = 7$  days. The initial Hanford detector is assumed in the simulations. The neutron star parameters are the same as in Figure 1. The lines shown in the diagrams correspond to the following models of the parameter space:  $f_o = 500$  Hz,  $\tau = 40$  yr,  $s_1 = 2$ ,  $s_2 = 1$ ,  $s_3 = 0$  (solid),  $f_o = 500$  Hz,  $\tau = 1000$  yr,  $s_1 = 1$ ,  $s_2 = 1$ ,  $s_3 = 0$  (dashed),  $f_o = 100$  Hz,  $\tau = 40$  yr,  $s_1 = 2$ ,  $s_2 = 1$ ,  $s_3 = 0$  (dotted),  $f_o = 100$  Hz,  $\tau = 1000$  yr,  $s_1 = 1$ ,  $s_2 = 1$ ,  $s_3 = 0$  (dotted/dashed). The dimensionless amplitude of the waveform  $h_o = 1.1 \times 10^{-23}$  for the models with  $f_o = 500$  Hz and  $h_o = 4.2 \times 10^{-25}$  for the models with  $f_o = 100$  Hz. On the two top panels the lines which correspond to the models with the same frequency  $f_o$  coincide.

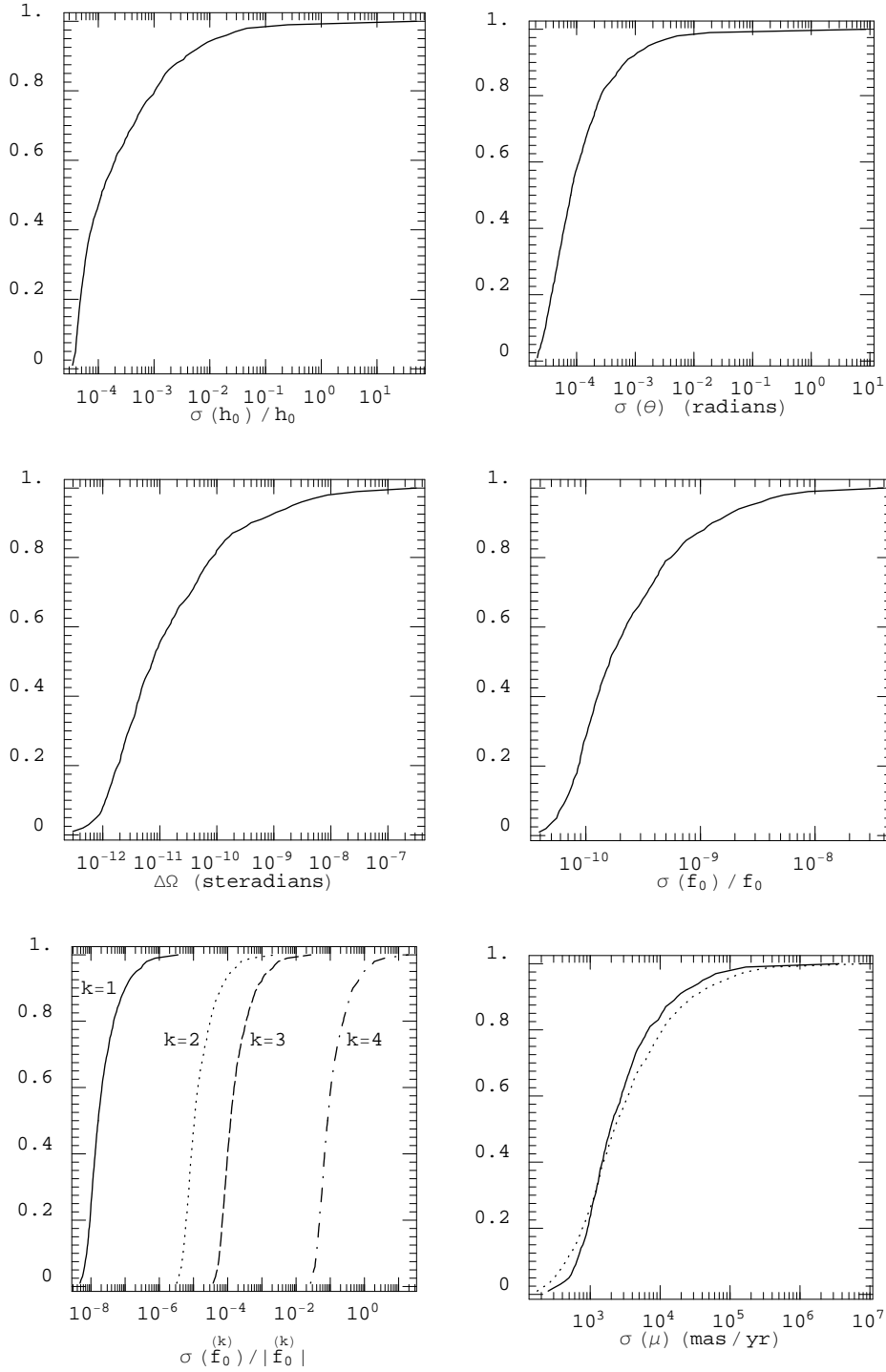


Figure 7: Cumulative distribution functions of the simulated rms errors of the signal parameters for all-sky searches including the two proper motion parameters  $\mu_\alpha$  and  $\mu_\delta$ . The observation time  $T_o = 120$  days. The advanced Hanford detector was taken in the simulation. We assume that star's ellipticity  $\epsilon = 10^{-5}$ , its moment of inertia w.r.t. the rotation axis  $I = 10^{45}$  g cm<sup>2</sup>, its distance from the Earth  $r_o = 40$  pc, and the frequency  $f_o = 500$  Hz [these values give the dimensionless amplitude of the waveform  $h_o = 2.6 \times 10^{-22}$ ]. The spindown age  $\tau = 40$  years. We have assumed that neutron star transverse velocity is  $10^3$  km/s. In the bottom right panel we give the distributions of the rms errors  $\sigma(\mu_\alpha)$  (solid) and  $\sigma(\mu_\delta)$  (dotted).

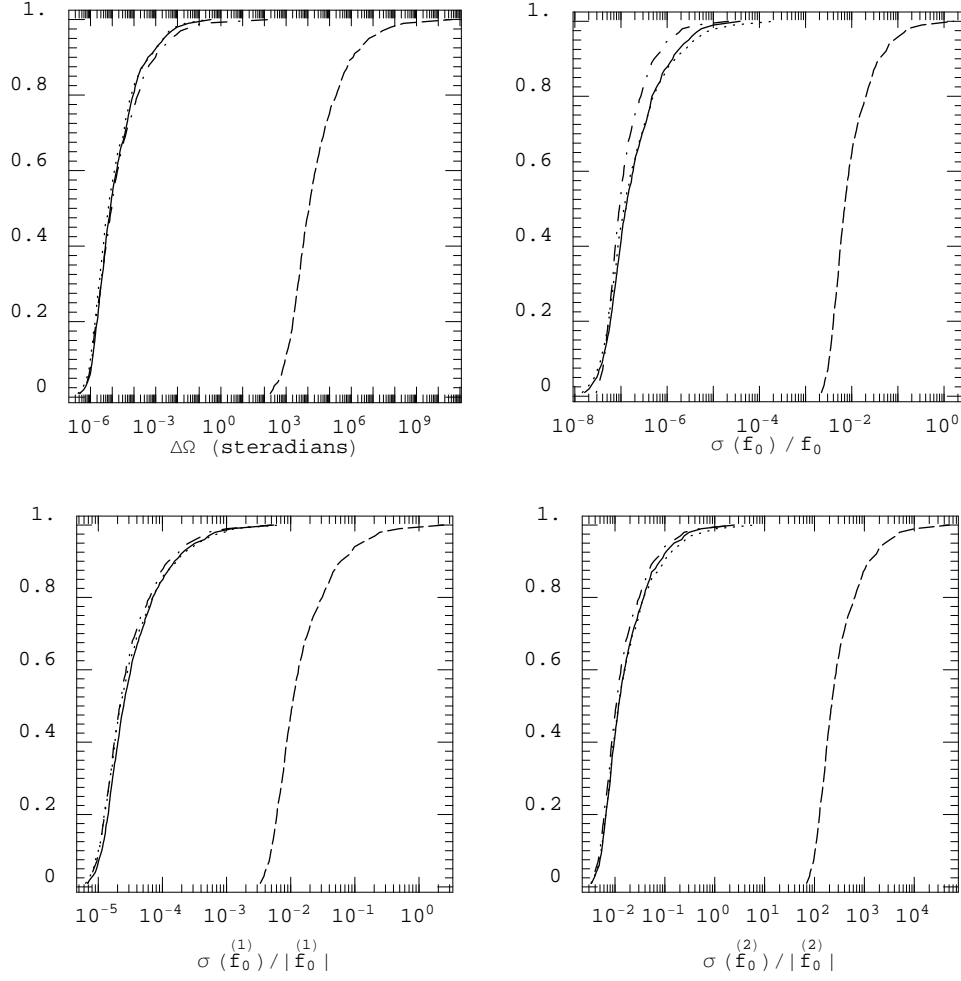


Figure 8: Comparison of cumulative distribution functions of the simulated rms errors of the signal parameters in the case of all-sky searches for the three simplified models of the gravitational-wave signal with the signal model given in Section 2. The observation time  $T_o = 7$  days. The initial Hanford detector is assumed in the simulations. The neutron star parameters are the same as in Figure 1 so the solid lines are the same as solid lines in Figure 1. The other lines are as follows: the constant amplitude model (dotted), the linear model I (dotted/dashed), and the linear model II (dashed).

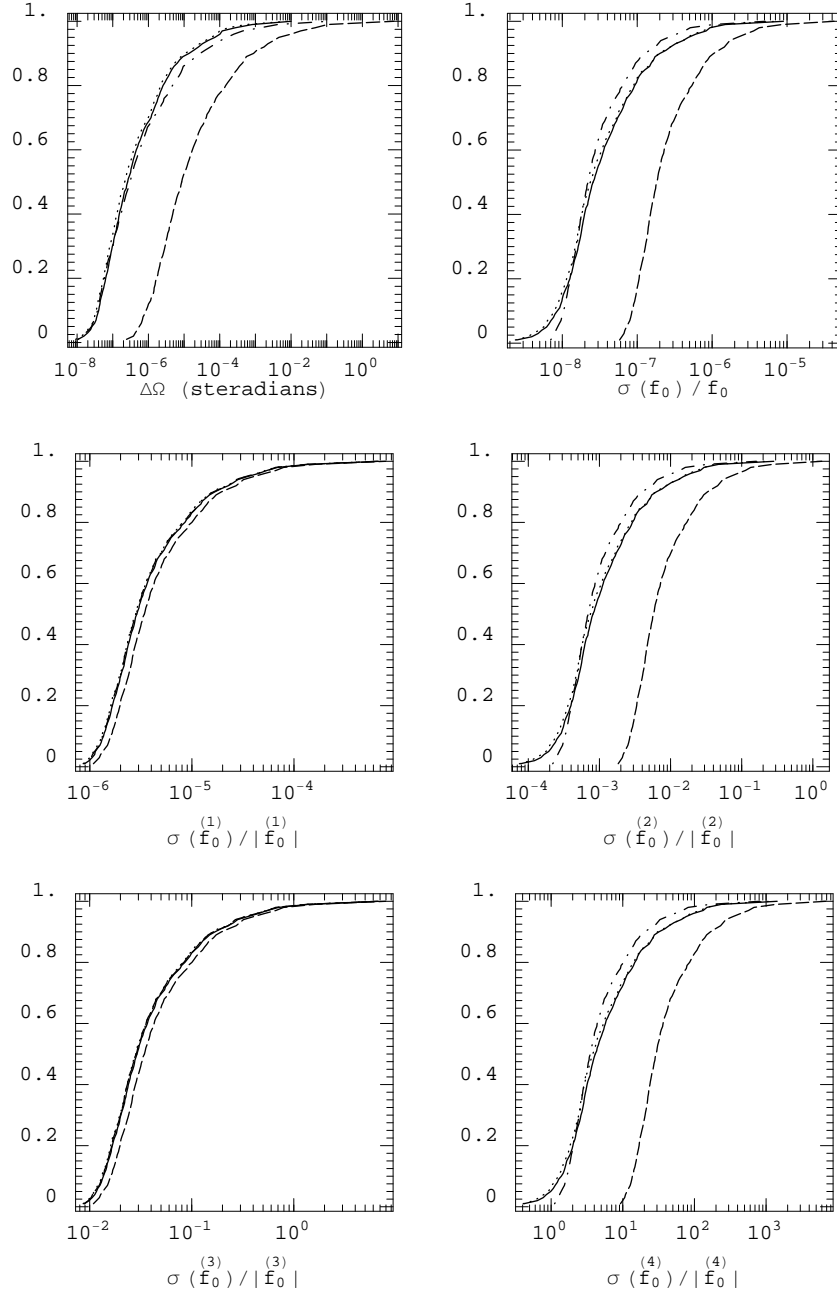


Figure 9: Comparison of cumulative distribution functions of the simulated rms errors of the signal parameters in the case of all-sky searches for the three simplified models of the gravitational-wave signal with signal model given in Section 2. The observation time  $T_o = 120$  days. The initial Hanford detector is assumed in the simulations. The neutron star parameters are the same as in Figure 1 so the solid lines are the same as solid lines in Figure 1. The other lines are as follows: the constant amplitude model (dotted), the linear model I (dotted/dashed), and the linear model II (dashed).

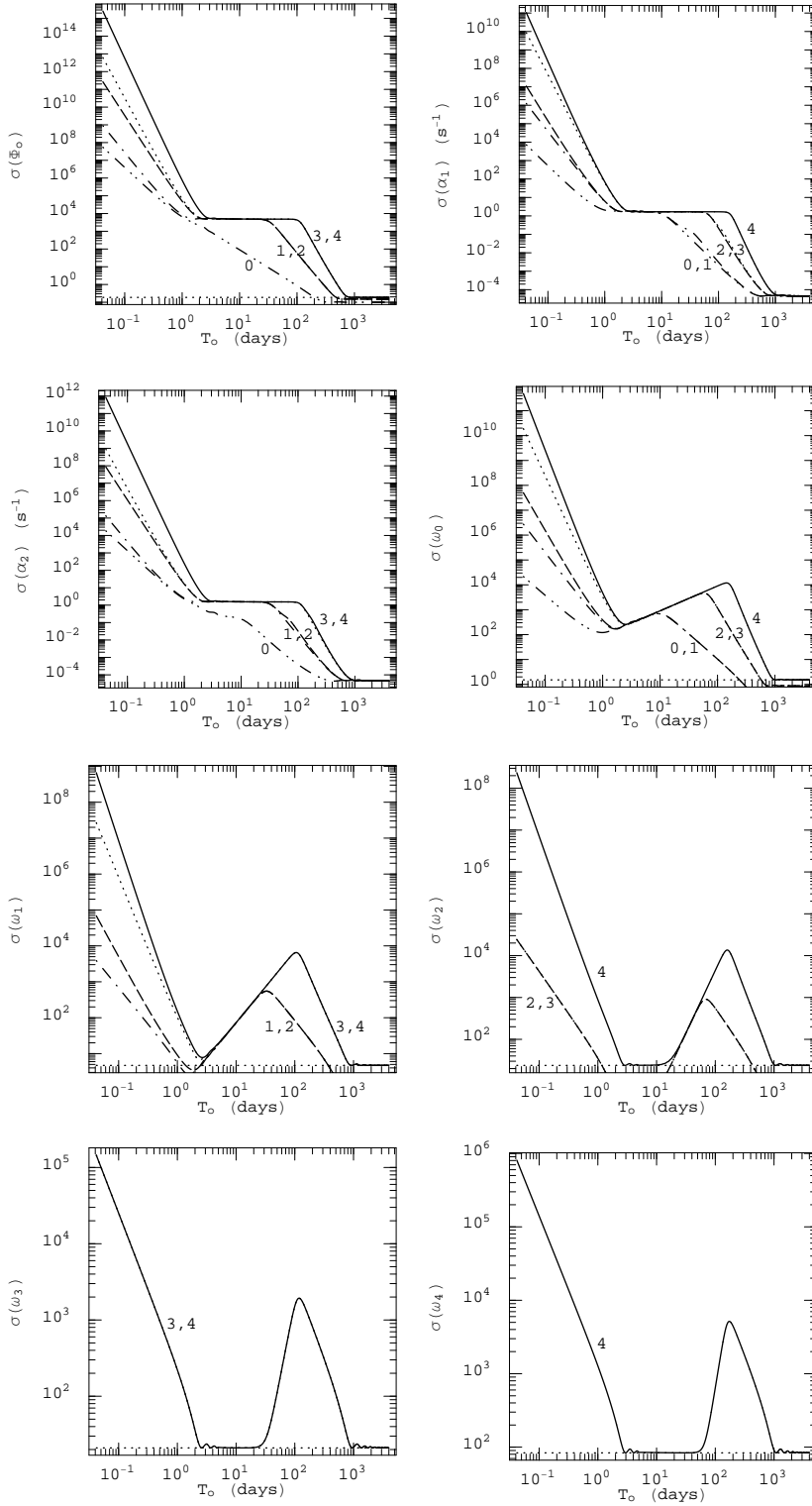


Figure 10: Dependence of the rms errors of the phase parameters on the observation time  $T_o$ . We have used the constant amplitude linear phase signal defined in Eqs. (57) and (58). The signal-to-noise ratio  $d = 10$ . We have assumed the latitude  $\lambda$  of the Hanford LIGO detector, we have also put  $\phi_r = 1.456$  and  $\phi_o = 0.123$ . The lines (and the numbers) in the diagrams correspond to different numbers  $s$  of spindown parameters included in the phase (58):  $s = 4$  (solid),  $s = 3$  (dotted),  $s = 2$  (dashed),  $s = 1$  (dotted/dashed), and  $s = 0$  (double dotted/dashed). The horizontal dotted lines give the rms errors of the parameters as predicted by the polynomial phase model with  $s = 4$  spindowns included (see Appendix C). The numbers corresponding to these lines are taken from Table 4 of Appendix C (for the signal-to-noise ratio  $d = 10$ ). We see that for the observation times  $T_o \gtrsim 1000$  days the horizontal lines coincide with the solid lines.

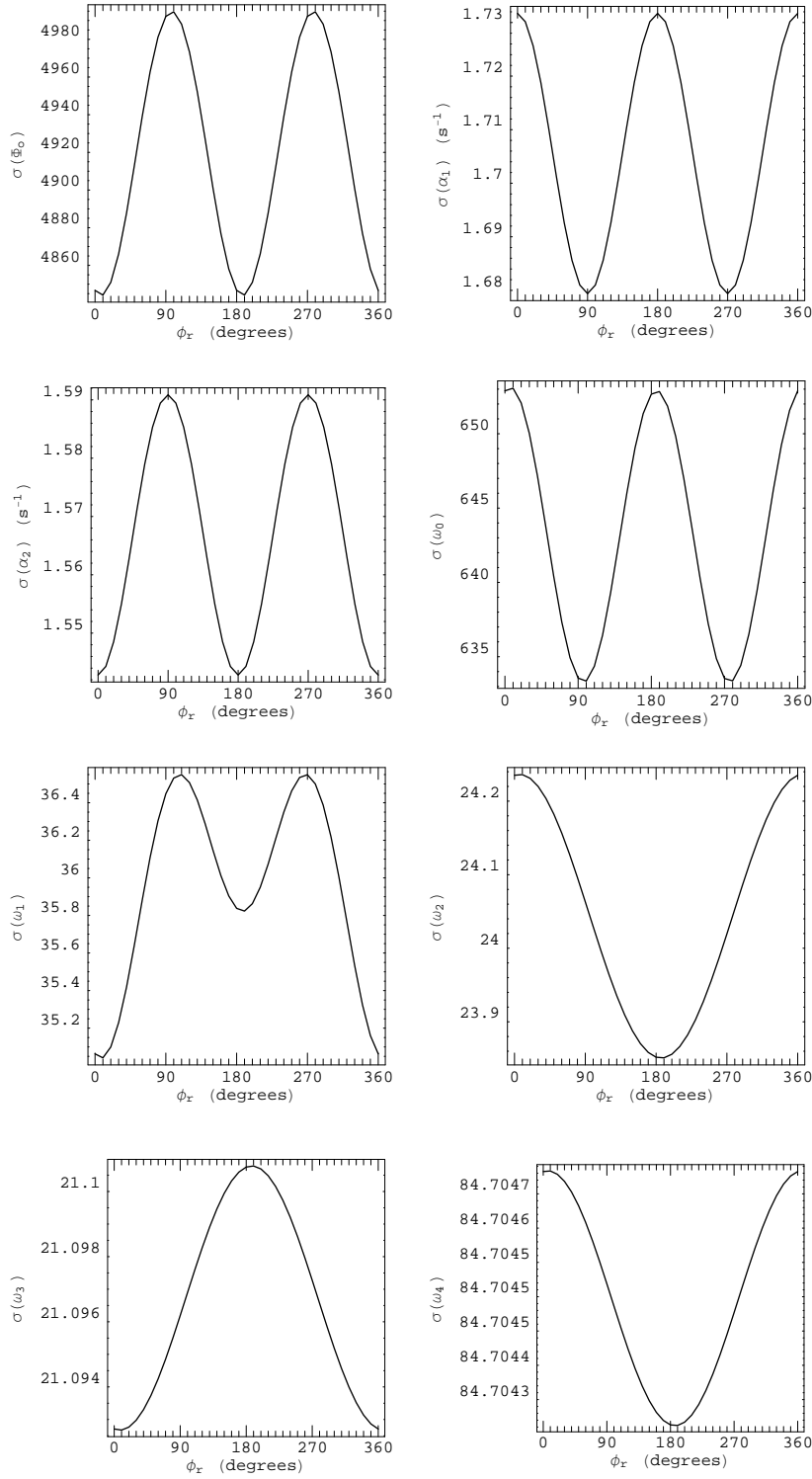


Figure 11: Dependence of the rms errors of the phase parameters on the initial phase  $\phi_r$  of the Earth's diurnal motion. We have used the constant amplitude linear phase signal defined in Eqs. (57) and (58) with  $s = 4$  spindown parameters included. The observation time  $T_o = 7$  days and the signal-to-noise ratio  $d = 10$ . We have assumed the latitude  $\lambda$  of the Hanford LIGO detector, we have also put  $\phi_o = 0.123$ .

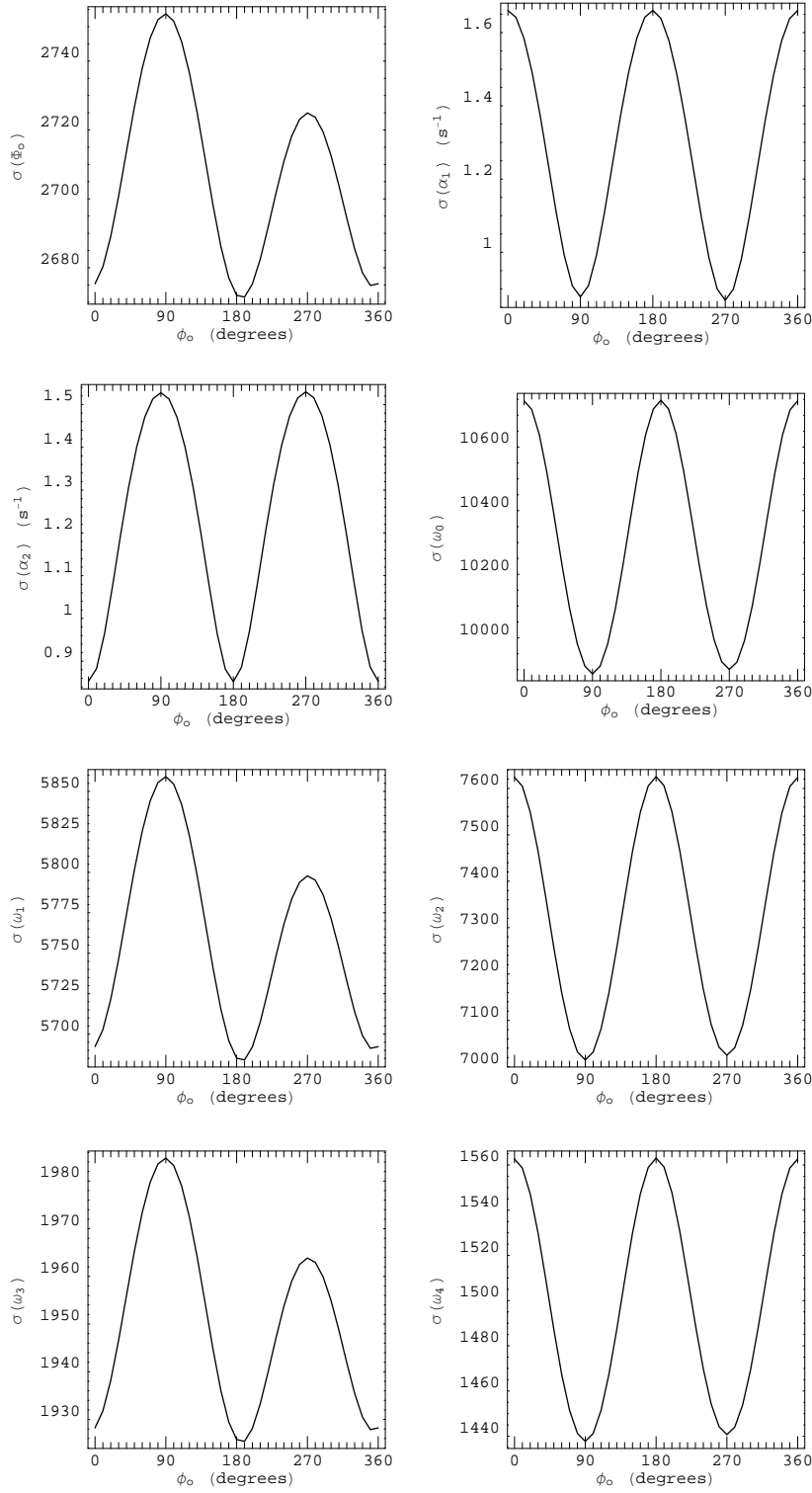


Figure 12: Dependence of the rms errors of the phase parameters on the initial phase  $\phi_o$  of the Earth's orbital motion. We have used the constant amplitude linear phase signal defined in Eqs. (57) and (58) with  $s = 4$  spindown parameters included. The observation time  $T_o = 120$  days and the signal-to-noise ratio  $d = 10$ . We have assumed the latitude  $\lambda$  of the Hanford LIGO detector, we have also put  $\phi_r = 1.456$ .

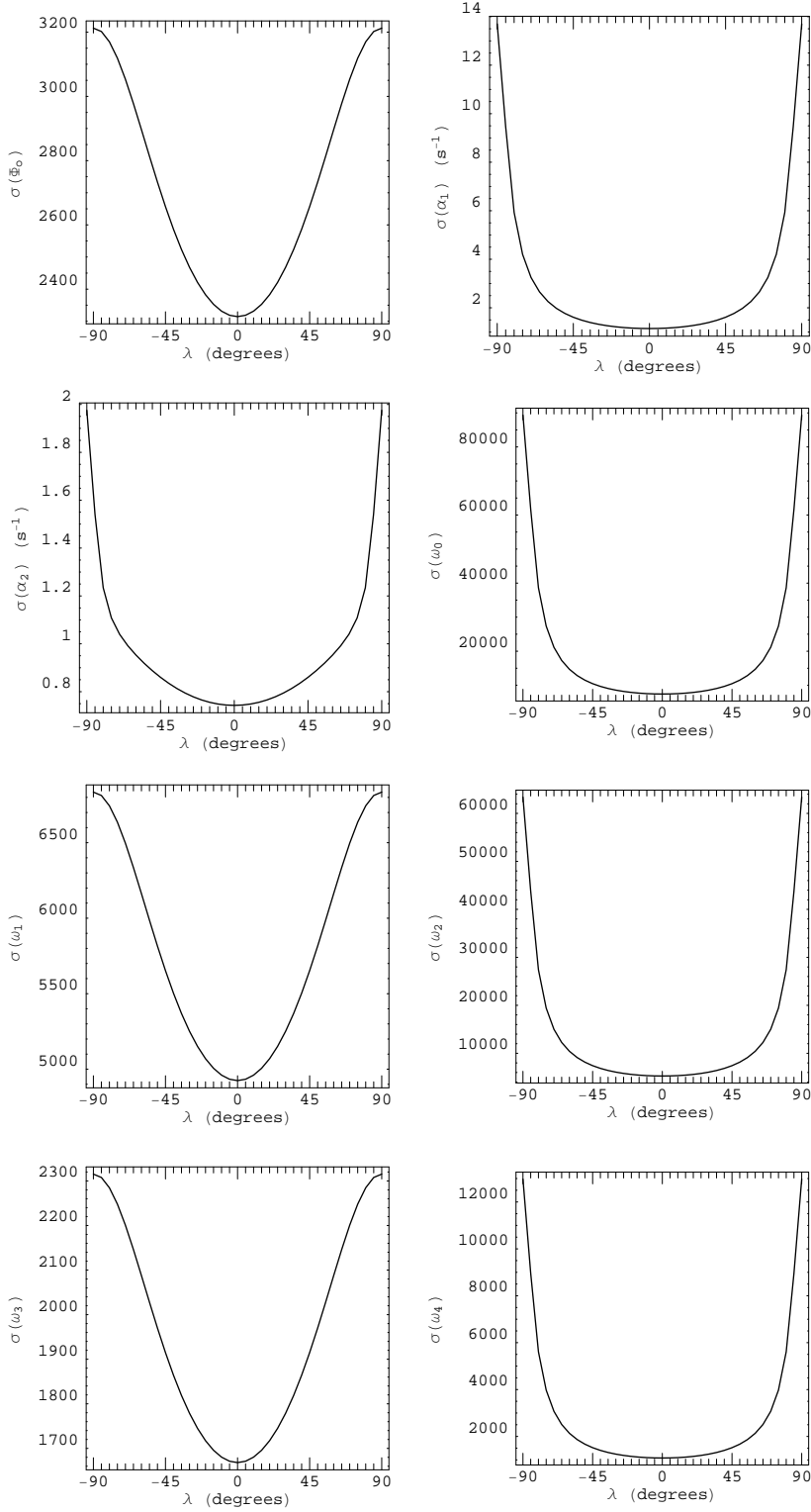


Figure 13: Dependence of the rms errors of the phase parameters on the latitude  $\lambda$  of the detector's location. We have used the constant amplitude linear phase signal defined in Eqs. (57) and (58) with  $s = 4$  spindown parameters included. The observation time  $T_o = 120$  days and the signal-to-noise ratio  $d = 10$ . We have put  $\phi_r = 1.456$  and  $\phi_o = 0.123$ .



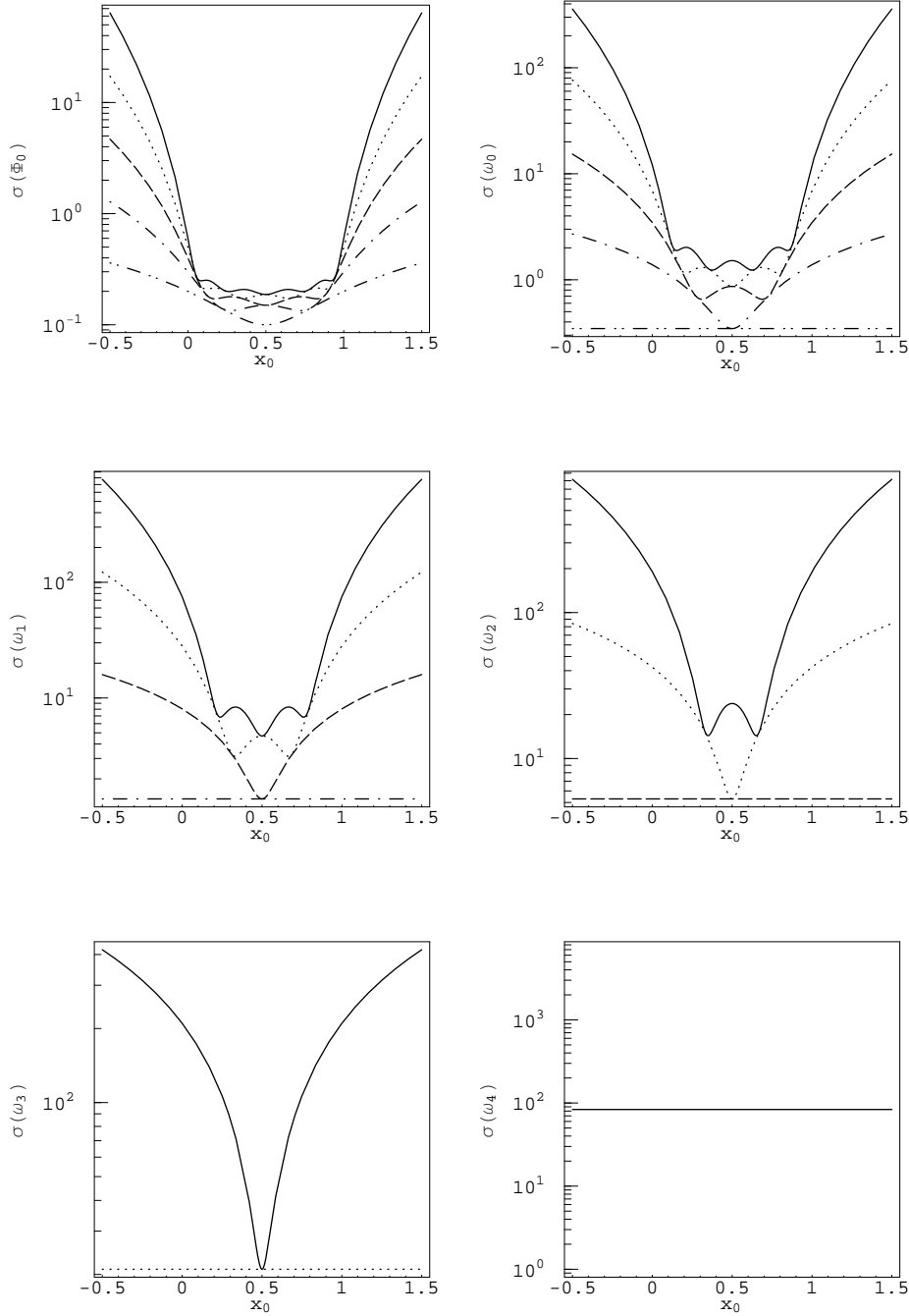


Figure 14: The rms errors  $\sigma(\zeta_k)$  of the phase parameters  $\zeta = (\Phi_0, \omega_0, \dots, \omega_4)$  plotted as functions of the initial time  $x_0$  for the signal-to-noise ratio  $d = 10$ . The curves correspond to models of the phase with increasing number of spindown parameters: dashed/double dotted curve—no spindown parameter (this corresponds to a monochromatic signal with unknown constant initial phase), dashed/dotted curve—1 spindown parameter, dashed curve—2 spindown parameters, dotted—3 spindown parameters, solid—4 spindown parameters. All the curves shown here are symmetric w.r.t.  $x_0 = 0.5$ . For some discrete values of  $x_0$  curves for  $(r + 1)$ -parameter model intersect with  $r$ -parameter model curves. This means that in such cases adding  $r + 1$  parameter does not change the rms error in  $r$ th parameter.

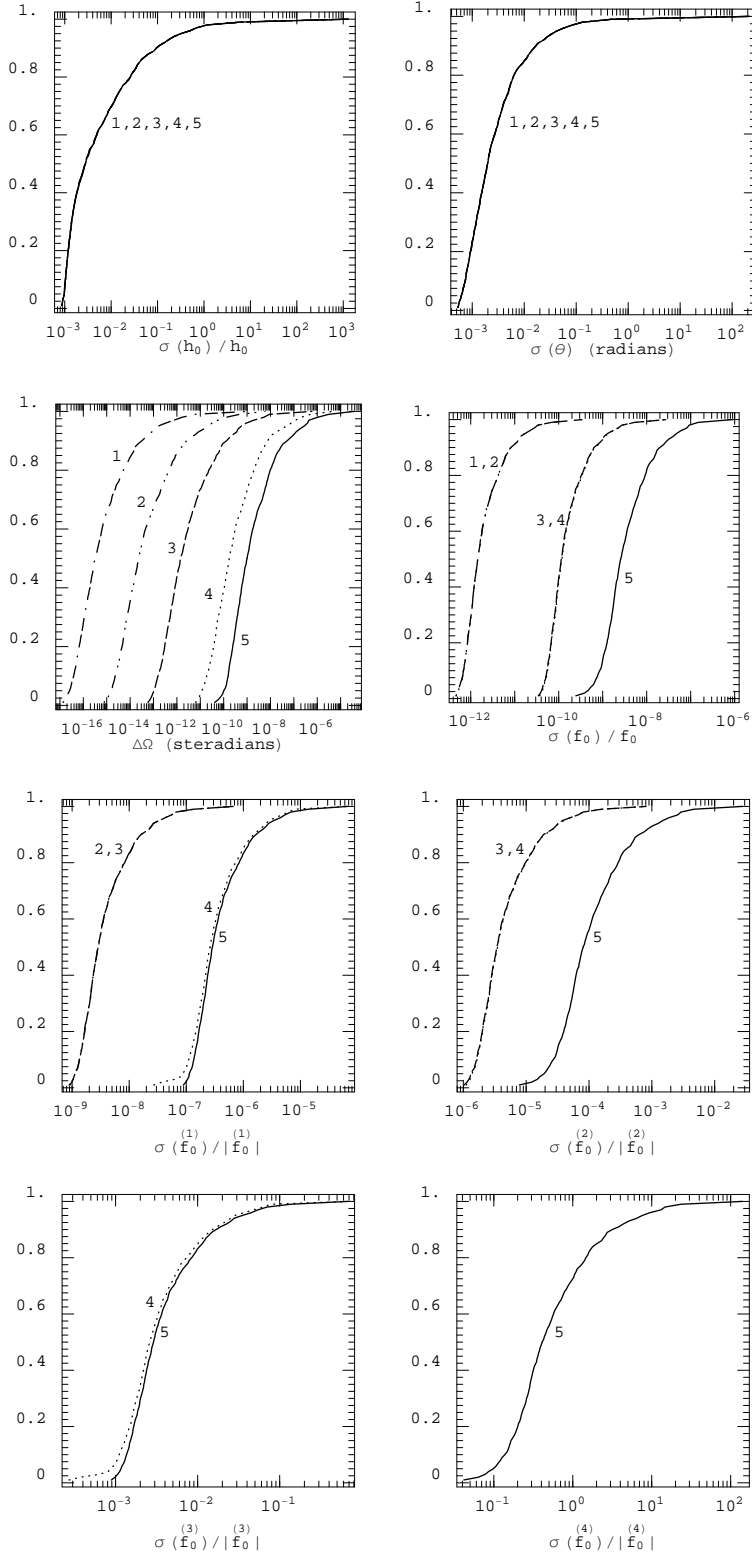


Figure 15: Cumulative distribution functions of the simulated rms errors of the signal parameters for all-sky searches. The observation time  $T_o = 120$  days. The advanced Hanford detector is assumed in the simulations. The neutron star parameters are the same as in Figure 1. For these set of parameters the model of the signal's phase consistent with the  $1/4$  of a cycle criterion is obtained from Eq. (12) by setting  $s_1 = 4$ ,  $s_2 = 3$ , and  $s_3 = 0$ . This is the model number 5 in the plots given here. Models 1 through 4 are defined as follows: model 4— $s_1 = 3$ ,  $s_2 = 3$ ,  $s_3 = 0$ ; model 3— $s_1 = 2$ ,  $s_2 = 2$ ,  $s_3 = 0$ ; model 2— $s_1 = 1$ ,  $s_2 = 1$ ,  $s_3 = 0$ ; model 1— $s_1 = 0$ ,  $s_2 = 0$ ,  $s_3 = 0$ . We observe a curve merging of the various models that corresponds exactly to the intersection points of the curves in Figure 14 for  $x_o = 0.5$ . This shows that qualitative properties of the Fisher matrix for the polynomial model are preserved in the exact model. The five cumulative distributions of the amplitude parameters in the two top panels are indistinguishable. This confirms an effective decorrelation of the amplitude and the phase parameters.